Bay Area Environmental Research Institute
560 Third Street West
Sonoma, CA 95476

FINAL TECHNICAL REPORT

Time period: March 1, 1999 through February 28, 2002

Project: Grant NCC 2-1105: In Situ Measurements of N2O and CH4 during SOLVE on the ER-2 using a new tunable diode laser instrument

Principal Investigator: Dr. Hans Jurg Jost

Date: May 9, 2002

TABLE OF CONTENTS

TABLE OF CONTENTS

I Introduction

This report is the final report for Cooperative Agreement NCC 2-1105: "In Situ Measurements of N2O and CH4 during SOLVE on the ER-2 using a new tunable diode laser instrument." The tasks outlined in the proposal are listed below with a brief comment. The publications and the conference presentations are listed. Finally the important publications are attached.

The Cooperative Agreement made possible a research effort to produce high precision and high accuracy *in situ* measurements of methane and nitrous oxide on the ER-2 during the SOLVE field campaign and to analyze these measurements. These measurements of CH4 and N2O were of utmost importance to studies of the ozone losses in the Arctic winter and spring. The concentrations measured over a large spatial and temporal range allowed the separation of the dynamical and chemical ozone loss.

The most important results of the SOLVE program were contained in two scientific papers (attached). This Cooperative Agreement allowed the participation of the Argus instrument in the program and the analysis of the data.

II. NCC 2 1105 Tasks and Accomplishments

The main tasks relating to the participation of the Argus instrument in SOLVE were as follows:

Task 1: Perform intercomparisons of the different instruments on balloon, DC-8, and ER-2 platforms measuring the same species as our instrument.

Task 2: Assess the subsidence in the Arctic vortex, specifically in conjunction with measurements aboard the ER-2 payload.

Task 3: Study the dynamical history of the air masses sampled during the mission, especially with theory groups who calculate trajectories.

Task 4: Investigate small scale structures observed in profiles to improve our understanding of exchange of intra- and extra polar vortex air. Previous studies focused mainly on the analysis of ozone depleted air observed outside the vortex.

Task 5: Investigate seasonal, interannual and interhemispheric change and differences in N2O and CH4, using the long time series of ATLAS N2O measurements.

Task 6: Study the N2O:NOy correlations to investigate denitrification.

Task 7: Quantify the O3 loss due to chemistry by helping to estimate the initial ozone using correlations with long live tracers (e.g., N2O).

Task 8: Use the CH4 measurements and H2O to investigate the occurence of dehydration in the Arctic.

In addition the following necessary tasks relating to the maintenance of the instrument and the laboratory were performed:

Task 9. Maintenance and upgrading of the Argus airborne instrument

- 9.1 Maintain Argus calibrations (ISO 9000 protocols)
- 9.2 Maintain Argus spares
- 9.3 Maintain Argus field support infrastructure
- 9.4 Define Argus upgrades
- 9.5 Argus documentation (ISO 9000)
- 9.6 GSE and software operational maintenance and upgrades

Task 10. Specific tasks to support lab infrastructure

- 10.1 Maintain ESD capability/training (ISO 9000)
- 10.2 Maintain electronic schematics (OrCAD software)
- 10.3 Integrate LabView data acquisition into lab laser operations optical bench
- 10.4 Maintain lab safety plan/haz-mat handling (ISO 9000 and HazMat regulations)

III. Publications:

1. D.W. Fahey, R.S. Gao, K.S. Carslaw, J. Kettleborough, P.J. Popp, M.J. Northway, J.C. Holecek, S.C. Ciciora, R.J. McLaughlin, T.L. Thompson, R.H. Winkler, D.G. Baumgardner, B. Gandrud, P.O. Wennberg, S. Dhaniyala, K. McKinney, Th. Peter, R.J. Salawitch, T.P. Bui, J.W. Elkins, C.R. Webster, E.L. Atlas, **H. Jost,** J.C. Wilson, R.L. Herman, A. Kleinbohl, and M. vonKonig, The Detection of Large HNO3-Containing Particles in the Winter Arctic Stratosphere, **Science,** Feb 9 2001: 1026-1031.

2. Popp, P.J.; Northway, M.J.; Holecek, J.C.; Gao, R.S.; Fahey, D.W.; Elkins, J.W.; Hurst, D.F.; Romashkin, P.A.; Toon, G.C.; Sen, B.; Schauffler, S.M.; Salawitch, R.J.; Webster, C.R.; Herman, R.L.; **Jost, H.;** Bui, T.P.; Newman, P.A.; Lait, L.R."Severe and Extensive Denitrification in the 1999-2000 Arctic Winter Stratosphere", **Geophys. Res. Lett** Vol. 28, No. 15, p. 2875,2001

3. Jost, H., M. Loewenstein, Argus: A Lightweight TDL Instrument to Measure Stratospheric Tracers, Application of Tunable Diode and Other Infrared Sources for Atmospheric Studies and Industrial Processing Monitoring II, SPIE annual meeting, Denver 1999.

IV Presentations

1. H. Jost, *et al,* "Mixing events during SOLVE/THESEO revealed by Tracer correlations" Annual Meeting of the Amer. Geophys. Union, December 2000, San Francisco, CA

2. Jost, H., *et al.,* Evidence for transport events into the tropical middle Stratosphere, AGU spring meeting, Washington DC, 2000.

3. Greenblatt, B.J., **H. Jost** *et al,*. Vortex Conditions in the Arctic Winter Stratosphere in 1999-2000: ER-2 Argus and Balloon LACE Tracer", AGU spring meeting, Washington DC, 2000.

PROCEEDINGS OF SPIE REPRINT

SPIE—The International Society for Optical Engineering

Reprinted from

Application of Tunable Diode and Other Infrared Sources for Atmospheric Studies and Industrial Processing Monitoring II

19–20 July 1999
Denver, Colorado

Volume 3758

Argus: A Lightweight TDL Instrument to Measure Stratospheric Tracers

Hansjürg Jost* and Max Loewenstein
NASA Ames Research Center, Atmospheric Chemistry and Dynamics Branch, MS 245-5, Moffett Field CA 94035, USA

ABSTRACT

Argus is a two channel, tunable diode laser instrument which measures atmospheric methane and nitrous oxide in the upper troposphere and stratosphere up to an altitude of 32 km using second harmonic detection. Investigations of stratospheric transport from mid-latitudes into the tropics is the current focus of our work which requires high precision and high accuracy data. Argus was designed for use on remotely piloted aircraft or light-payload balloons and weighs less than 20 kg. The two channels each have their own laser, optics, detector and signal processing chains. We sample methane at 3.3 μm and nitrous oxide at 4.5 μm at a rate of 0.1 Hz. The gas is sampled in a Herriott cell which has a total path length of 18.8 m. Each laser is current- and temperature-controlled by a dedicated microprocessor. We sweep the laser at 10 Hz and record direct absorption spectra during the ramping of the laser current. The lasers are modulated with a 40 kHz sine wave; a phase sensitive amplifier and integrator detects the second harmonic data. The analysis is performed offline by applying direct fits to the measured spectra using the non-linear Marquardt-Levenberg algorithm. We have recently flown Argus and ATLAS together on the ER-2 platform for comparison. Precision of Argus is 0.6% and accuracy is estimated to 4-17% increasing with altitude.

Keywords: atmospheric tracers, second harmonic detection, stratosphere, methane, nitrous oxide

1. INTRODUCTION

High accuracy and precision measurements of trace gases in the atmosphere allow us to investigate transport of air masses. In the stratosphere (10-45km above ground), relatively long lived tracers, like nitrous oxide (N_2O), methane (CH_4), Carbon Dioxide (CO_2) or certain CFC's, contain information about the transport processes, because their lifetime is long compared to typical transport time scales. Both methane and nitrous oxide have sources in the troposphere and sinks in the stratosphere. At these altitudes the primary source of N_2O is from air entering the stratosphere with a mixing ratio of about 315 ppbv with no annual cycle and a long term increase of 0.3% per year. In the stratosphere N_2O on average decreases monotonically with increasing altitude due to UV photolysis (wavelengths below 230 nm) and because of its low chemical reactivity N_2O has no other significant sink in the lower stratosphere. The lower stratospheric lifetime of N_2O is long compared to vertical and horizontal transport time scales[1]. Methane also has its primary source in the troposphere and enters the stratosphere with a mixing ratio of about 1.7 ppmv. Its decrease with increasing altitude is dominated by oxidation with OH and $O(^1D)$ with minor contribution from reaction with Cl. Its photochemical lifetime ranges from over a hundred years at 20 km to a few months at 40 km, which is long compared to the transport time constants (≈ weeks)[1]. Instead of investigating profiles of tracers, their correlation contains very useful information. The correlation of N_2O and CH_4 with other species is often found to be very compact or even linear. As has been explained by Plumb and Ko [2], compact and linear relationships between tracers is found as long as the tracers are long lived relative to vertical transport time. The compact relationships last, although not linear, as long as the chemical lifetimes are still long compared to horizontal transport times. Inversely, if the correlation in the tropics differs from that measured at mid-latitude, the assumption of rapid mixing of the air masses seem to be violated and we can infer the effectiveness of the dynamical barrier, the so called tropical pipe[2,3]. Observation of laminae with exceptional correlations in the tropics can give us insight into the short term mixing of air masses from mid-latitudes into the tropics[4]. All these investigations require high accuracy and precision measurements of trace gases.

In search of a new high altitude research platform, the National Aeronautics and Space Administration (NASA) initiated work in the early 1990's on the Perseus-A remotely piloted aircraft (RPA). As this platform had quite severe restrictions on payload weight and size, the need for small, lightweight *in-situ* instruments for atmospheric research came up. Argus, named in reference to the Greek multi-eyed creature because it measures several species (methane and nitrous oxide), was designed and realized for the Perseus-A vehicle. Due to delays in the RPA project, Argus was deployed on a balloon payload. Together with five other tracer instruments it forms the Observation of Middle Stratosphere (OMS) payload. Within about

* Correspondence: Email: hjost@mail.arc.nasa.gov; phone 650 604 0697; fax 650 604 3625

Part of the SPIE Conference on Application of Tunable Diode and Other Infrared Sources for Atmospheric Studies and Industrial Processing Monitoring II • Denver, Colorado • July 1999
SPIE Vol. 3758 • 0277-786X/99/$10.00

1.5 hours the 113,000 m³ helium filled balloon rises to 32 km and is then slowly valved down before the payload is separated from the balloon and lands on a parachute. The total payload weighs about 600 kg and has been retrieved with minor or no damage after each of the seven flights. OMS has been deployed successfully from Northeastern Brazil, New Mexico and Alaska.

Argus is an evolution from the very successful Airborne Tunable Laser Absorption Spectrometer (ATLAS)[5]. ATLAS is a single channel, diode laser instrument for nitrous oxide operating on the NASA ER-2 aircraft during many airborne field campaigns like the Airborne Antarctic Ozone Expedition (AAOE, 1987), or more recently the Stratospheric Tracers of Atmospheric Transport (STRAT, 1995-1997) and the Photochemistry of Ozone Loss in the Arctic Region in Summer (POLARIS,1997). ATLAS measures the N_2O amount by forming the second harmonic peak ratio to a NIST traceable standard gas, whereas Argus records full spectra and uses spectroscopic line parameters to determine the gas amount.

2. ARGUS INSTRUMENT DESCRIPTION

2.1 Mechanical Configuration

Argus in its current configuration, weighs about 20 kg and the main dimensions are 40cm x 30cm x 30 cm. The shroud, made out of fiber glass honeycomb and fiber glass facings, encloses the optics, electronics and sample cell. The pump, pump controller, calibration system and the platform interface box are mounted separately. A schematic is shown in Figure 1. The turbo pump is controlled to draw a constant flow of ambient air through the sample cell. The platform interface collects the Global Positioning System (GPS) signal provided by the balloon platform and transfers instrument data to the telemetry transmitter.

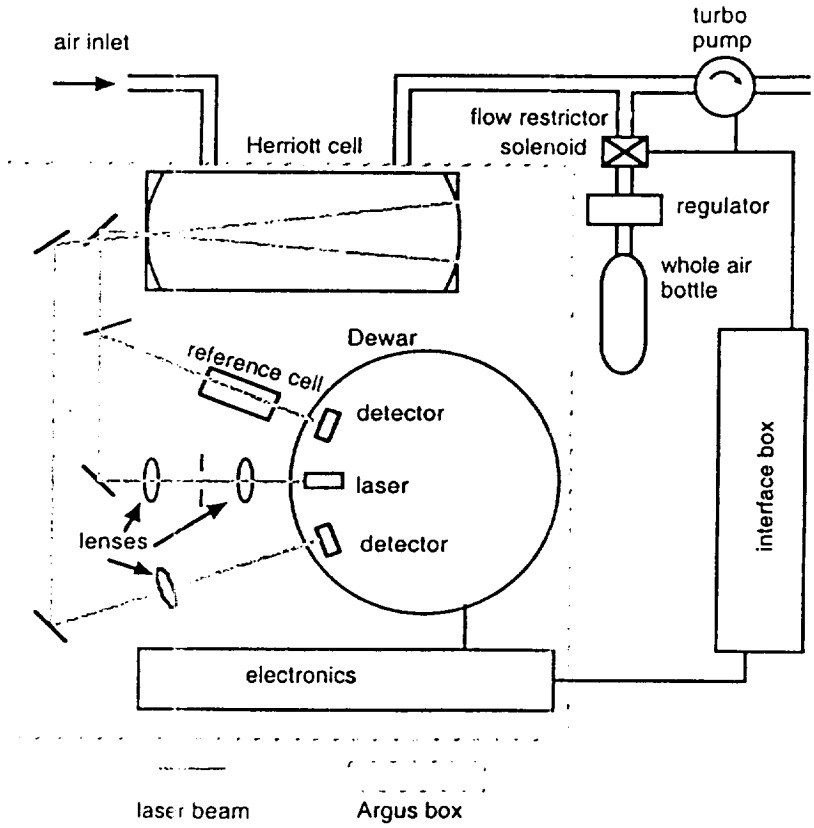

Figure 1: Schematic of Argus

Inside the shroud, there are two main platforms. The lower level accommodates the electronics, electrical distribution, inlet gas heater and the MKS pressure transducer. Mounted on shock absorbers on top is the optical table, a honey comb composite structure. The aluminum dewar extends into the lower level and holds 1.8 liters of liquid nitrogen lasting for 10 hours of operation and 30 hours idle. To reduce warping of the table a custom shaped heater is mounted to the underside and

a PID control loop keeps the temperature at 30 °C. The electronics are kept at ambient pressure, as well as all the other components contained in the instrument box. Copper heat sinks have been glued onto the processors and other hot spots to prevent overheating due to the lack of convective air cooling at altitude where the air density is reduced to about 1% of an atmosphere. These heat sinks transfer the heat to the electronic chassis bottom and from there a 2.5cm aluminum bar connects to a radiation panel that also serves as a physical protection at landing.

2.2 Optical Design

The two channels each have their own laser, optics and detectors. Both channels have the same layout and are separated vertically. Only one is shown in Figure 1; they lie on top of each other in this perspective. We currently use lead salt diode lasers to measure methane in the ν_3-band at 3.3μm and nitrous oxide in the ν_3-band at 4.5μm. The diodes, along with 4 indium antimonide (InSb) detectors, are mounted in a single custom liquid nitrogen dewar.
The f/1 diode laser beam is shaped to a quasi-collimated f/40 beam using two 1/2 inch diameter zinc sulfide lenses. At the intermediate focus is a pin hole to stop additional spatial modes a laser might have. All lenses and windows are anti-reflection coated with reflection less than 0.3%.
A 10:1 beam splitter couples part of the laser beam through a reference cell to the dedicated reference detector. We use the well known spacing of absorption lines for the frequency calibration of the atmospheric spectra. The nitrous oxide channel reference cell contains CO and N_2O and we employ the CO R17 and N_2O P19 spacing which is 0.305 cm^{-1}, the methane reference cell contains $^{12}CH_4$ and isotopic $^{13}CH_4$ and we use the R0 spacing which is 0.100 cm^{-1}, respectively. Additionally, the reference spectral line shapes are used for instrument performance monitoring in flight.
The beam passes 72 times through a 26 cm base path length Herriott cell for a total path of 18.8m. The ambient inlet air is preheated to 30°C.
Currently the signal to noise of the instrument is limited by fringe patterns. The fringe spacing indicates reflecting surfaces separated by twice the Herriott cell length and we successfully reduced the fringe size by thermally modulating the walls of the Herriott cell, even though we were not yet able to identify the scattering sources that produce the dominant fringe.

2.3 Electrical Design

Figure 2 gives a simplified overview of the electronic design. We use the rapid scan method and second harmonic detection[6]. A first digital to analog converter (DAC) sets the bias current of the laser diode. We sweep the laser at 10 Hz and record direct absorption spectra during the ramping of the laser current. A ramp consists of 1024 discrete points controlled by the ramp DAC. To determine the detector dark current, the laser is chopped by turning the bias current off during the first 24 steps of the ramp. A synthesized 40 kHz sine wave modulation is superimposed on the ramp by a third DAC. The sum of the 3 DAC signals drives a transistor that provides the laser current. The detector signal is amplified with a preamplifier and a programmable gain amplifier adjusts the signal within the dynamic range of the analog to digital converter (ADC). The phase sensitive amplifier demodulates at 80 kHz using a digital signal provided by the field programmable gate array (FPGA). An integrator is reset at the beginning of each ramp step and integrates during the four full cycles of the fundamental modulation frequency. The integrator signal is then digitized by an ADC. Due to the weight and size constraints we use stacked custom PC104 cards. Each laser is independently controlled by the FPGA, which initiates bias, ramp and modulation. Temperature is controlled by a channel-dedicated 386 microprocessor, which also coadds the spectra and communicates with the host processor. We attain an RMS temperature stability of about 5 mK using diodes as sensing elements. To maximize the 2f peak amplitude the sample modulation amplitude is continuously adjusted to 2.2 times the Voigt width of the absorption feature[7]. We coadd 100 signal ramps before storing them, corresponding to a 0.1 Hz sample rate. A full cycle of spectra consists of 2s coadded direct sample absorption, 10 s second harmonic sample absorption and 2s each of reference direct and second harmonic spectra.

A third microprocessor, the host, running DOS operating system, controls the overall system and optics temperatures, serves an ethernet port which connects to the ground support computer, and saves the recorded spectra and housekeeping data to a solid state disk. Pressure in the sample cell is measured with two transducers: One with low accuracy for the range of 0-1000 mbar, the other for 0-130 mbar with an accuracy of 1% of full scale. During the flight, the data is transmitted to the ground using a 19200 baud radio link.
The electronics are exposed to ambient pressure and the heat is dissipated from a radiation panel connected to the electronics through a heat-conducting bar, as mentioned earlier.

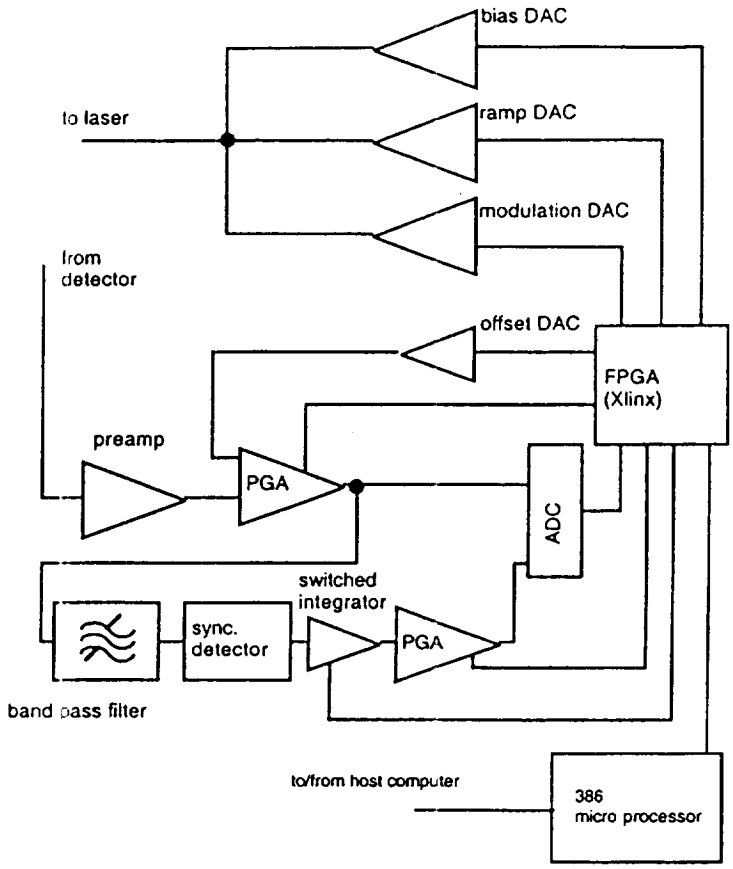

Figure 2: simplified schematic of laser drive electronic and signal detection for one channel.

2.4 Inflight Calibration system

We have recently added an inflight calibration system to Argus that is based on a 1 liter gas tank filled with a NOAA Climate Monitoring and Dynamics Laboratory (CMDL) certified whole air containing 313.6 ppb N_2O and 1766.3 ppb CH_4. A regulator and a needle valve serving as a restrictor supply a flow that is twice as large as the flow provided by the pump. When the calibration system is activated by opening a solenoid, the cal gas flow back flushes the sample cell within a few seconds.This design makes sure that we don't get any contamination of the sample flow by leaks out of the calibration system, except if the solenoid fails. In this case the limited calibration gas supply will stop after a few minutes and undisturbed ambient measurements resume. The calibration system is activated 4 to 6 times for about two minutes during a flight by sending a start and a stop command over the telemetry. In the data analysis, the calibrations are not specially marked because the activation of the calibration system is independent of the instrument operation. We generally do not use the in-flight calibration data to correct the ambient concentrations, but to validate the full set of laboratory calibrations with a partial set during the flight and to estimate our accuracy.

3. Instrument Calibration and Preparation

In preparation for and after a flight we perform a calibration of the instrument at several pressures and mixing ratios. Whole air certified to 2% by NOAA/CMDL is flow mixed with blow off from a liquid nitrogen tank which proved to be a good zero gas for N_2O and CH_4. The flow mixing is controlled by measuring the flow of the calibration tank and using a metering valve on the zero gas to attain a certain mixing ratio. A full set of calibration consists of 1 minute each of 100 %, 75%, 50%, 25% of whole air at a pressure of 130 mbar, 100 mbar, 70 mbar, 40 mbar, 25 mbar and 12 mbar. At each pressure we perform a linear least square fit to the retrieved volume mixing ratios to determine the calibration factor. Typical 1 σ standard deviation of the slope is 1%. From the reference cell data we determine the instrument contribution to the Gaussian broadening of the lines

and can compare it to the reference cell Doppler width retrieved during a flight. A saturation cell is inserted in the laser beam to check the single mode quality of the laser and the current and temperature set points are adjusted for minimal transmission. We deliberately detune the temperature by as much as 0.3 K to check for laser mode breaks close to our desired lines and tune the set points to be centered between them. With a 3 cm long germanium etalon we monitor the frequency tuning of the laser and found it to be linear to better than 1 percent, which allows us to derive the frequency axes of our spectra by simply using the spacing of two line absorptions in the reference cell.

4. Data Analysis

After recovery of the flash disk from the instrument we analyze the data off-line. Telemetry data are used for first looks and could be used as a fall back in case of a catastrophic landing. In a first step the 2f spectra are gain normalized and divided by the corresponding direct spectra. For frequency calibration we use spectra from the reference cells.
Direct fits of the second harmonic component of a sine modulated Voigt function are applied to the preprocessed spectra using the non-linear Marquardt-Levenberg algorithm[7]. This method is smoothly varying between an inverse-Hessian (close to the minimum) and steepest descent (far from the minimum). We fit a total of 7 parameters: the line position, slope and offset of the baseline, number density, Lorentz and Doppler width and the modulation amplitude. A typical spectrum and fit is shown in Figure 3. We found that we could reduce the sensitivity to residual fringe patterns in the spectra by fixing both Lorentz and Doppler width. We calculate the Lorentz width from the measured pressure using the pressure broadening parameter from the HITRAN 96 spectroscopic database. For the Doppler width we use the mean value found by fitting the reference second harmonic spectra. In the postprocessing fits with too large chi square, too high number of iterations, too small signal to fringe ratio, or spectra with a high laser temperature change relative to the preceding spectrum are omitted from the final data. The algorithm is implemented in Interactive Data Language (IDL™) and run on a Silicon Graphics workstation.

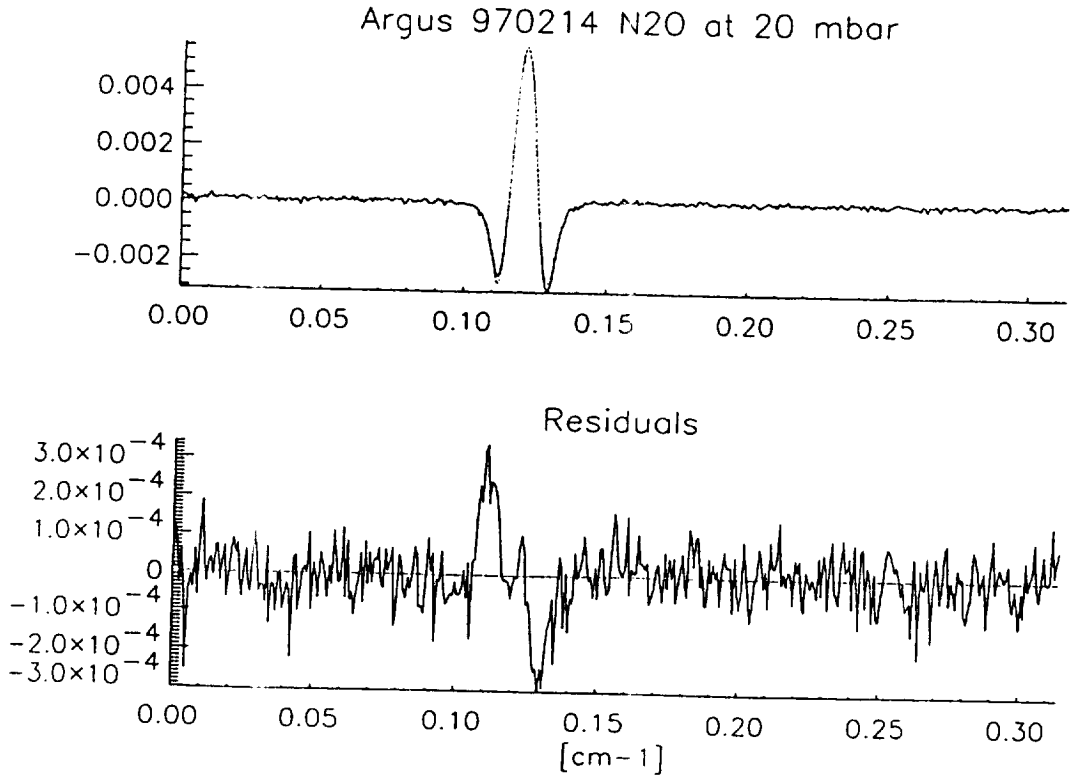

Figure 3: Top: typical spectrum measured during the 970214 flight in Juazeiro do Norte, Brazil, 7°S and result of non-linear fit. Bottom: Difference between calculated and measured spectrum shown in top portion.

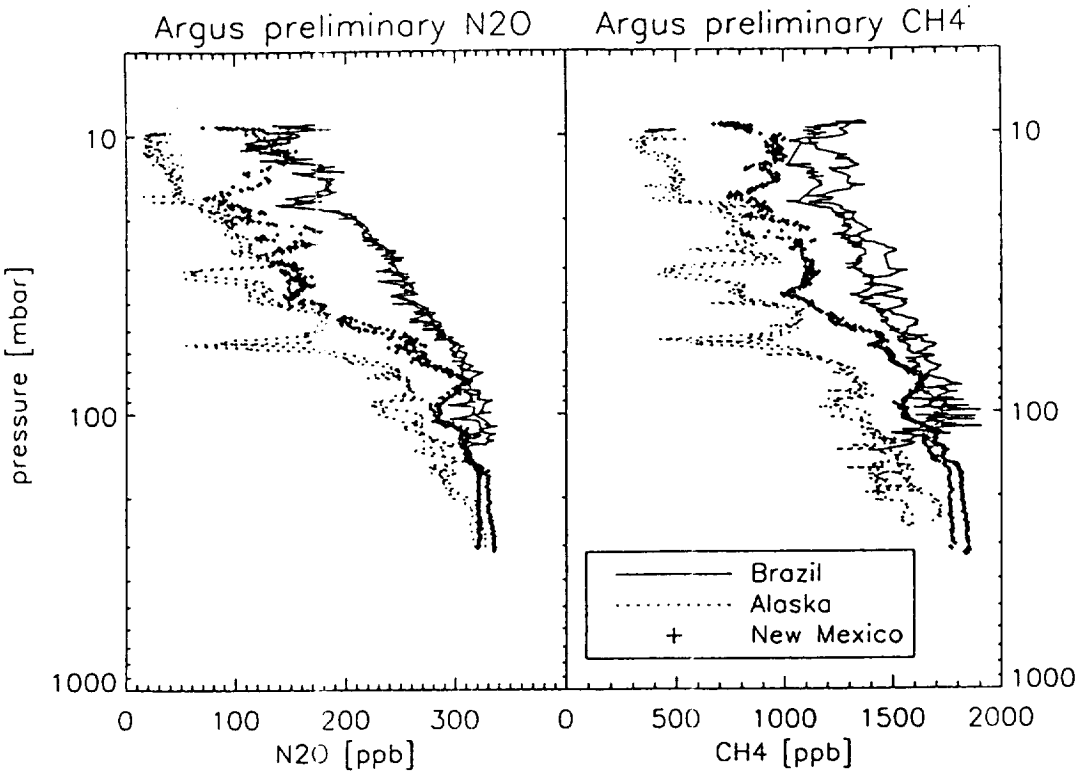

Figure 4: Profiles measured with Argus in Juazeiro do norte, Brazil 971111 (7°S), Fort Sumner, New Mexico, 980518 (31°N) and Fairbanks, Alaska, 970630 (64°N)

5. Results

Argus has been deployed on the OMS payload out of Fort Sumner, NM, on 960610, 960921 and 980518 (format YYMMDD), Juazeiro do norte, Brazil, on 970214, 971111 and 971120, and Fairbanks, AK, on 970630. Data representing tropical data from Brazil, mid-latitude from Fort Sumner and high latitudes from Alaska are shown in Figure 4. The profiles are not very smooth, but have thin laminae (thickness less than 1 km) with depleted N_2O and CH_4. In the Arctic, these laminae have been attributed to remnants of the polar vortex which broke up more than 2 month earlier[3]. In the tropical data, the laminae are recent intrusions of mid-latitude air and their age can be estimated from the ozone recovery to typical tropical values at the observed altitudes[4]. In Table 1 an overview of the error budget is shown for 980518.The largest contribution is from the pressure transducer (accuracy: 1% of full scale (130mbar)) and can be up to 16% at 8 mbar, but of course decreases

	channel 1	channel 2
Source	relative error in VMR (%)	relative error in VMR (%)
Gamma_d	1-3	n/a
Calibration Standard	2	2
Calibration Slope	1.2	4.2
Pressure	0.4-16	0.4-16
Total (RMS)	2.6-16	4.7-17

Table 1: accuracy error budget of Argus for 980518.

rapidly with increasing pressure. The calibration slope is determined from the pre- and post-flight laboratory calibration runs. For channel 2 we had a discrepancy in the two calibrations slopes and this reflected in the higher percentage error. Gamma_d reflects the uncertainty in the Gaussian line width contribution from the instrument. In November 98 we flew ATLAS and Argus together on the ER-2. Argus was run in a slightly different mode than on the balloon: For the signal second harmonic we co-added only 20 ramps before storing them, hence increasing the data rate to 0.5 Hz. The in-flight calibration system was not easily adaptable for the ER-2 and hence not used.

From the preliminary data analysis, we found that Argus currently has a 1% precision in flight at 50 mbar for 2s data and 0.6% for 10s data. From the differences to ATLAS we estimate the current accuracy at 50 mbar was 4-5%. A flight segment with data from Argus and ATLAS is shown in Figure 5. These result are in good agreement with a comparison of ER-2 and OMS balloon instruments during coincident measurements in Alaska (S. Alex, Harvard University, personal communication).

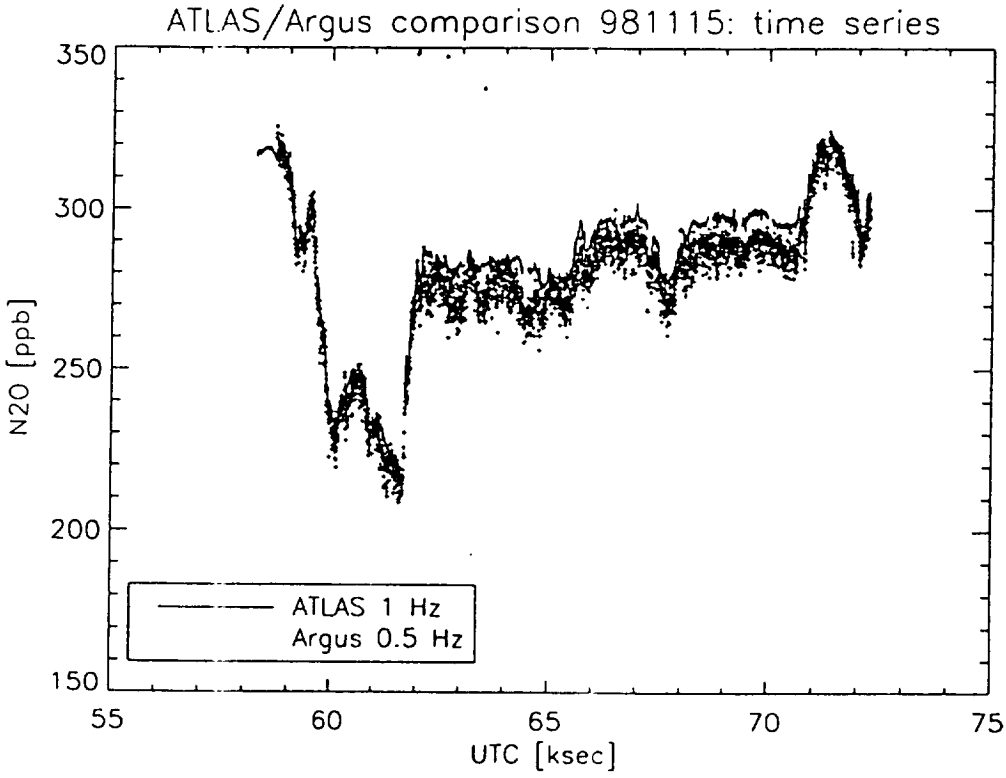

Figure 5: Time series of simultaneous measurements of N_2O of Argus and ATLAS aboard the ER-2 in November 1998.

6. Future Modifications and Plans

Our next field mission will be aboard the NASA ER-2 airplane during the NASA SAGE Ozone Loss and Validation Experiment (SOLVE). We plan to permanently adapt Argus for the ER-2 by changing the heat management to a forced air, convective cooling system. We will improve some key electronic components in the harmonic detection to reduce electronic noise. The laser temperature stability will be increased by switching from diode sensors to resistive elements and therefore reducing the temperature noise due to the AM detection by the diodes of high frequency signals radiated by the digital electronics. A major improvement of the precision down to 0.5% is expected by using a 36 m astigmatic Herriott cell, essentially doubling the path length. Further we will improve the data analysis for the aircraft environment, and increase the data rate to 0.5 Hz. An extensive intercomparison of N_2O instruments, including ATLAS, in September 1999 will allow determination of the accuracy and precision of the modified Argus and assure the continuation of the ATLAS data series. With all these efforts we expect to reduce the accuracyof Argus to 2-3%.

ACKNOWLEDGMENTS

This project is funded by the NASA ERAST program, the NASA Aeronautics directorate (High Speed Research program) and the Mission to Planet Earth (MTPE, Atmospheric Effect of Stratospheric Aircraft program). We would like to thank Jeff Grose, Peter Sharer, Angela Bulat Wahab, Scott Jensen, Nghia Mai and John Marmie for their support in the field missions. This work was partially performed while H. Jost held a National Research Council Associateship at NASA Ames Research Center.

REFERENCES

1. G. Brasseur and S. Solomon, *Aeronomy of the Middle Atmosphere*, D. Reidel Pub. Co.; Norwell, MA, 1986.
2. R.A. Plumb and M.K.W. Ko, "Interrelationships between mixing ratios of long-lived stratospheric constituents", *J. Geophys. Res,*.**97**, pp. 10145-10156, 1992
3. C. M. Volk, et al., "Quantifying transport between the tropical and mid-latitude lower stratosphere", *Science*, pp. 1763-1768, 1996
4. H. Jost, M. Loewenstein, L. Pfister, J. J. Margitan, A. Y. Chang, R. J. Salawitch, H. A. Michelsen, "Laminae in the tropical middle stratosphere: Origin and age estimation", *Geophys. Res. Lett*, **25**, pp 4337-4340, 1998.
5. Podolske, J. R. and Loewenstein, "Airborne tunable diode laser spectrometer for trace-gas measurement in the lower stratosphere", *Appl. Opt.*, pp 5324-5333, 1993.
6. J. Reid and D. Labrie,"Second-harmonic detection with tunable diode lasers - comparison of experiment and theory" *Appl. Phys.B* **26**, pp. 203-210, 1981
7. W.H. Press, S. A. Teukolsky, W.T. Vetterling, Brian P. Flannery, *Numerical Reipes*, second edition, Cambridge University Press, Cambridge, 1992
8. R. Herman, et al, "Tropical entrainment time scales inferred from stratospheric N_2O and CH_4 observatoins", *Geophys. Res. Lett.*, **25**, pp 2781-2784, 1998

of virtual walls, we can produce functionality on microchips that is difficult to realize by other methods. For example, concentrating samples in microfluidic systems is nontrivial. Methods reported include sample stacking using "isoelectric focusing" (*30*) and on-chip solid phase extraction (*31*). The virtual walls provide an intuitive method to concentrate liquids on microchips. Virtual walls can also mimic the function of lungs by exchanging components between liquid and gas phases. In combination with in situ–constructed stimuli-responsive hydrogel components (*25, 32*), more complex functions could be added to realize even greater control in microfluidic systems. We believe that the approaches we describe provide enhanced functionality and design flexibility that expand the toolbox for the design and fabrication of microfluidic systems.

References and Notes

1. M. Freemantle, *Chem. Eng. News* 77 (no. 8), 27 (1999).
2. M. A. Unger *et al.*, *Science* **288**, 113 (2000); J. Fahrenberg *et al.*, *J. Micromech. Microeng.* **5**, 169 (1995); C. Goll *et al.*, *J. Micromech. Microeng.* **6**, 77 (1996); X. Yang, C. Grosjean, Y. C. Tai, C. M. Ho, *Sens. Actuators A* **64**, 101 (1998).
3. D. J. Harrison *et al.*, *Science* **261**, 895 (1993).
4. H. Salimi-Moosavi, T. Tang, D. J. Harrison, *J. Am. Chem. Soc.* **119**, 8716 (1997).
5. G. Beni, M. A. Tenan, *J. Appl. Phys.* **52**, 6011 (1981).
6. B. S. Gallardo *et al.*, *Science* **283**, 57 (1999).
7. D. E. Kataoka, S. M. Troian, *Nature* **402**, 794 (1999).
8. M. A. Burns *et al.*, *Proc. Natl. Acad. Sci. U.S.A.* **93**, 5556 (1996).
9. A. W. Adamson, *Physical Chemistry of Surfaces* (Wiley, New York, ed. 5, 1990).
10. J. C. Mcdonald *et al.*, *Electrophoresis* **21**, 27 (2000).
11. K. Handique, B. P. Gogoi, D. T. Burke, C. H. Mastrangelo, M. A. Burns, *Proc. SPIE* **3224**, 185 (1997).
12. E. Delamarche, A. Bernard, H. Schmid, B. Michel, H. Biebuyck, *Science* **276**, 779 (1997).
13. K. Ichimura, S.-K. Oh, M. Nakagawa, *Science* **288**, 1624 (2000).
14. H. Gau, S. Herminghaus, P. Lenz, R. Lipowsky, *Science* **283**, 46 (1999).
15. A. A. Darhuber, S. M. Troian, S. M. Miller, *J. Appl. Phys.* **87**, 7768 (2000).
16. A. D. Strook *et al.*, *Phys. Rev. Lett.* **84**, 3314 (2000).
17. G. T. A. Kovacs, *Micromachined Transducer Sourcebook* (McGraw-Hill, Boston, 1998).
18. B. H. Weigl, P. Yager, *Science* **283**, 346 (1999).
19. P. J. A. Kenis, R. F. Ismagilov, G. M. Whiteside, *Science* **285**, 83 (1999).
20. S. Takayama *et al.*, *Proc. Natl. Acad. Sci. U.S.A.* **96**, 5545 (1999).
21. A. Ulman, *An Introduction to Ultrathin Organic Films* (Academic Press, Boston, 1991).
22. A. Ulman, *Chem. Rev.* **96**, 1533 (1996).
23. B. Zhao, D. Mulkey, W. J. Brittain, Z. Chen, M. D. Foster, *Langmuir* **15**, 6856 (1999).
24. We used hexadecane (Aldrich, 99%) as a solvent to form SAMs of trichlorosilanes on silica substrates. Contact angle measurement showed that SAMs with full coverages were formed on glass substrates in less than 2 min.
25. D. J. Beebe *et al.*, *Nature* **404**, 588 (2000).
26. Hexadecane and the solution of trichlorosilane in hexadecane [0.5 weight-to-volume percent (w/v %)] were pumped into channels by two syringe pumps (Harvard Apparatus PHD 2000 Programmable). Syringes were connected to pipette tips fixed to channels by silicone tubing (Helix Medical, 0.040" ID/ 0.085" OD). Because the reactivity of trichlorosilanes is high, solvent was always introduced into the channel before the silane solution to eliminate the formation of SAMs in unwanted areas. At the end of the process, flow of the silane solution was always halted before stopping the flow of pure solvent. The flow rates of solvent and solution were usually the same, either 1 or 2 ml/min; the flow time was 2 to 3 min. The channels were cleaned by sequentially flushing with 10 ml of hexane and 10 ml of methanol followed by drying with a stream of clean air or nitrogen.
27. A pipette tip with inner diameters of 8 mm at the bottom and 6 mm at the top was fixed onto the channels. The maximum pressure that virtual walls can withstand was determined by gradually adding deionized water into the pipette and then measuring water height when a bulge developed.
28. The surface free energy of Rhodamine B dilute solution is lower than that of deionized water, resulting in a lower maximum pressure.
29. D. H. Rich, S. K. Gurwara, *J. Am. Chem. Soc.* **97**, (1975); V. N. R. Pillai, *Synthesis (Germany)* (1980).
30. S. C. Jacobson, M. Ramsey, *Electrophoresis* **16**, (1995).
31. R. D. Oleschuk, L. L. Shultz-Lockyear, Y. Ning, Harrison, *Anal. Chem.* **72**, 585 (2000).
32. D. J. Beebe *et al.*, *Proc. Natl. Acad. Sci. USA* **97**, 13488 (2000).

33. Supported by a grant from the Defense Advanced Research Projects Agency (MTO F30602-00-2-0543) (A. Lee, Program Manager). We acknowledge [illegible] for assisting with the images and Q. Yu for generating the photomasks.

8 November 2000; accepted 4 January 2001

The Detection of Large HNO_3-Containing Particles in the Winter Arctic Stratosphere

D. W. Fahey,[1,3]* R. S. Gao,[1] K. S. Carslaw,[4] J. Kettleborough,[5] P. J. Popp,[1,3] M. J. Northway,[1,3] J. C. Holecek,[1,3] S. C. Ciciora,[1,3] R. J. McLaughlin,[1] T. L. Thompson,[1] R. H. Winkler,[1] D. G. Baumgardner,[6] B. Gandrud,[7] P. O. Wennberg,[8,9] S. Dhaniyala,[8] K. McKinney,[8] Th. Peter,[10] R. J. Salawitch,[11] T. P. Bui,[12] J. W. Elkins,[2] C. R. Webster,[11] E. L. Atlas,[7] H. Jost,[12,13] J. C. Wilson,[14] R. L. Herman,[11] A. Kleinböhl,[15] M. von König[15]

Large particles containing nitric acid (HNO_3) were observed in the 1999/2000 Arctic winter stratosphere. These in situ observations were made over a large altitude range (16 to 21 kilometers) and horizontal extent (1800 kilometers) on several airborne sampling flights during a period of several weeks. With diameters of 10 to 20 micrometers, these sedimenting particles have significant potential to denitrify the lower stratosphere. A microphysical model of nitric acid trihydrate particles is able to simulate the growth and sedimentation of these large sizes in the lower stratosphere, but the nucleation process is not yet known. Accurate modeling of the formation of these large particles is essential for understanding Arctic denitrification and predicting future Arctic ozone abundances.

Polar stratospheric cloud (PSC) particles play a well-recognized role in the chemical loss of stratospheric ozone over the Antarctic and Arctic regions in winter/early spring (*1–3*). PSCs are formed at low temperatures (<200 K), characteristic of the winter stratosphere, through the co-condensation of water and HNO_3. Heterogeneous reactions on PSC particles produce active chlorine species. The sedimentation of PSC particles irreversibly removes HNO_3 (denitrification) and water (dehydration) from the lower stratosphere. Denitrification slows the return of chlorine to its inactive forms and, hence, enhances ozone destruction in a winter/spring season (*4–6*).

Evidence of denitrification is abundant in both polar stratospheres from both in situ and remote observations (*2, 7–11*). Denitrification is most intense over the Antarctic region, where large fractions of available NO_y are irreversibly removed from the stratosphere each winter. NO_y is the sum of prin reactive nitrogen species, of which HN NO, NO_2, N_2O_5, and $ClONO_2$ are import in the lower stratosphere (*12*). In princi denitrification must involve the sedim tion of large HNO_3-containing particles (*14*), but important details of the proces not been confirmed by observation or described theoretically. The concentrati denitrifying particles must generally be less than that of the background liquid sul aerosols (0.1-μm diameter). Too little densable material (HNO_3, H_2O) exists stratosphere to allow all particles to simultaneously to sizes sufficient for sedimentation, particularly when ice does form.

Here we report observations in the winter stratosphere of a newly identified of large HNO_3-containing particles. The ticles were observed between January

particles contribute substantially to denitrification in the lower stratosphere? Third, how do these particles form in the lower stratosphere? To address the first question, we used a statistical simulation to determine the size and number concentration of particles sampled in interval 2 (Fig. 2). This 800-s interval was chosen because the average NO_y signal due to particles is large (21 ppbv) and has a relatively constant standard deviation. This suggests that the size distribution is also relatively invariant over this interval. The large-particle NO_y signal is defined as the difference between the front and rear NO_y values and thus only includes NO_y associated with particles larger than 2 μm (Fig. 2). The statistical simulation accounts for the sampling of more than one particle in any 1-s sampling period and for the spreading of HNO_3 from an individual particle over more than a single 1-s period (*20*). The NO_y time s simulated by sampling a randomly population of NAT particles along flight track (Fig. 3). The number tions in each size interval are the parameters. The representativenes size distribution was determined by ing the occurrence histogram of N ence values with that from the simu series (Fig. 3). The best-fit size di was found by iteratively adjusting bution to minimize the difference (Fig. 3B).

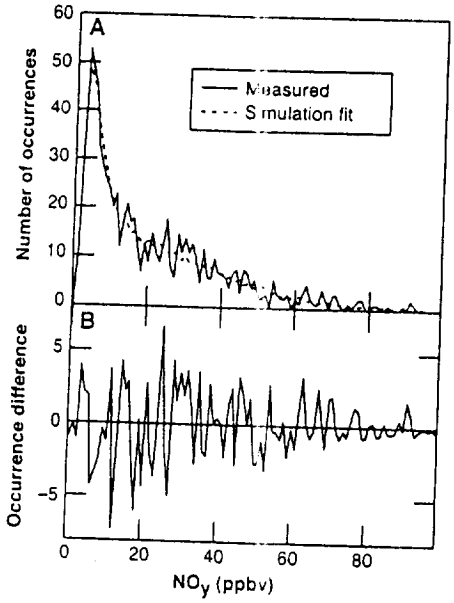

Fig. 3. Results from the statistical simulation of NO_y difference values for interval 2 on 20 January. The occurrence histogram of NO_y difference values is shown in (A) for the 800 s of observations in interval 2 (solid line) and for 20,000 s in the simulation (dashed line). The larger simulation period reduces the variability in the simulation histogram in (A). The best-fit size distribution for interval 2 is given by the Gaussian functions N (# cm^{-3} μm^{-1}) = 2.8×10^{-3} exp[−20(D − 3.5)^2] + 4.3×10^{-5} exp[−0.083(D − 14.5)^2], where D is the particle diameter in μm (Fig. 4). Gaussian functions are chosen for convenience to represent particle populations at large and small sizes. Lognormal distributions could also be used. The simulated time series is produced by superimposing the released HNO_3 from all particle sizes and averaging it to 1-s intervals to match the sampling period of the NO_y instrument. The differences between the simulated and observed histograms are shown in (B). The differences are very sensitive to the features of the large mode. For example, shifting the large mode by ±2 μm would produce significantly larger differences in (B) than shown. The small-size mode in Fig. 4 is required to match the histogram peak below 10 ppbv. The exact number and size of these smaller particles is more uncertain than for the larger particles. The small mode represents only a subset of particles present in the atmosphere below a 5-μm diameter. The histogram comparison is not sensitive to the presence of additional particles with sizes between the two size modes and with concentrations $<10^{-5}$ particles cm^{-3} μm^{-1}.

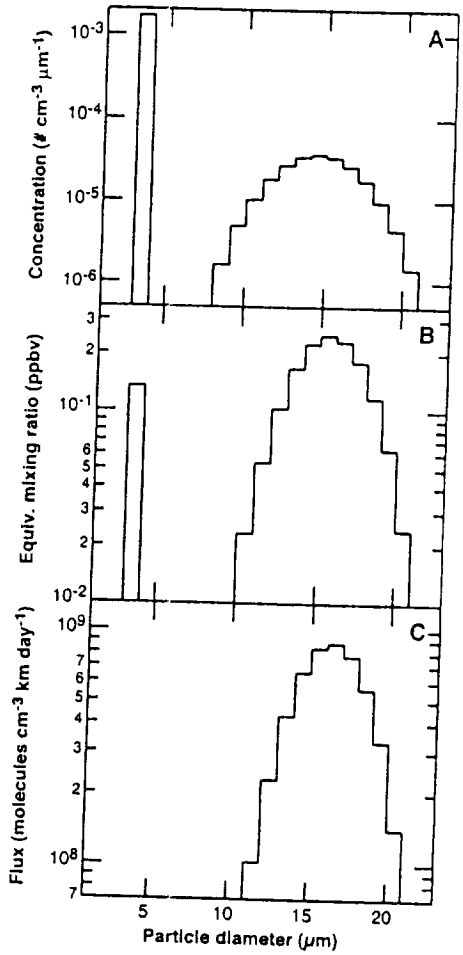

Fig. 4. Results from the statistical simulation of NO_y values in interval 2 on 20 January. Panels show (A) the adjusted best-fit size distribution and number concentration, (B) the equivalent gas-phase mixing ratio of HNO_3 derived from the distribution, and (C) the derived flux of HNO_3 at 60 hPa (~19.5 km). The size distribution is given by the Gaussian functions in the caption of Fig. 3 adjusted to account for size-dependent sampling efficiency. The adjustments, which are in addition to a basic particle enhancement factor of 12.8 (*12*), vary from +30 to −10% over the size range and are, calculated with a fluid dynamical model of the particle separator. The concentration integral of the large (small) mode is 2.3×10^{-4} cm^{-3} (2×10^{-3} cm^{-3}), with an estimated uncertainty of ±30%. The lower limit of the vertical axis in (A) corresponds to the detection of a single particle over the 800-s observation period. The total gas-phase HNO_3 of the large (small) mode is 1.5 ppbv (0.2 ppbv). The HNO_3 flux of the combined distribution is 5×10^9 molecules cm^{-3} km day^{-1} or 2.2 ppbv km day^{-1} at 60 hPa.

Two particle size modes, shown are required in our analysis to repro occurrence histogram of interval 2. T mode has a mean diameter of 14.5 μ total number concentration of 2.3 cm^{-3}. This mode produces most of values above 10 ppbv in Fig. 3. The mode at 3.5 μm has a number conce of ~2×10^{-3} cm^{-3} and is well s from the larger mode by size bins wit particles. For these concentrations, particle is sampled by the front inlet imately every 1.8 s, and a small pa sampled every 0.2 s on average. The mass contained in the large mode is lent to an ambient gas-phase value ppbv along the flight track (Fig. 4E mass of the more numerous smaller n ~0.2 ppbv. Because the simulation is difference between the two NO_y m ments, the small mode in Fig. 4 rep only the largest sizes in one or more p modes present in the atmosphere be diameter of 5 μm (*16*). With low speeds, these smaller modes form sep from the large-particle mode and nearer sampling altitude, and may include pa composed of STS.

To answer the second question, w these particles contribute substantial stratospheric denitrification, we note th existence of large HNO_3-containing pa means that denitrification has already curred because particles sediment durin growth process. An instantaneous sedim tion flux of HNO_3 can be calculated to simulated size distribution by convolvin fall speed and NO_y content for each pa size in 1-μm size intervals (Fig. 4C). T speed of a 14-μm spherical particle is km day^{-1} at 18 to 19 km (*21*). The H flux for interval 2 is 5×10^9 molecules km day^{-1} (2.6 ppbv km day^{-1}) at altitudes. The flux values for many flight intervals on 20 January are simila the basis of average NO_y difference and occurrence histograms for these in vals. Thus, some denitrification must occurred above flight altitudes in the vor before 20 January in order to produce large particles observed on that day in widely distributed air parcels. The denitri

cannot account for differences in observed particle number concentrations. Concentrations depend on the spatial and temporal variation of the particle nucleation process throughout the low-temperature regions of the vortex.

The sensitivity of large particle formation to available HNO_3 and temperatures near ice saturation was examined with a one-dimensional model of aerosol growth and sedimentation (Fig. 6) (*20*). The results show that the maximum NAT particle size that could be found at ER-2 cruise altitudes (50 to 70 hPa) is near 20 μm in diameter for average HNO_3 values observed above ER-2 altitudes in mid-January (7 to 9 ppbv) (*26*). This maximum size is consistent with the NO_y observations (Fig. 4). At ER-2 sampling altitudes, a 25% reduction in available HNO_3 causes a 10% reduction in particle size (20 to 18 μm). Similarly, a 2 K increase in temperature reduces the particle diameter by <10%. Particle sizes >22 μm can only be produced with a uniform abundance of >10 ppbv HNO_3 above the aircraft, which is greater than that observed in January to March 2000. These and larger particles were therefore unlikely to be found at or above a 60-hPa pressure altitude (~19 km).

The particle growth model results show that denitrification by large particles is mostly controlled by the kinetics of HNO_3 vapor deposition onto particles at conditions away from thermodynamic equilibrium of the NAT condensed phase. This is a result of the low number concentrations of particles and their large fall speeds. The assumption that NAT particles are in equilibrium, as used in various ways in most current atmospheric model simulations of denitrification, will lead to incorrect simulations of denitrification. Thus, the observations and analysis presented here suggest a need for fundamental changes in the vortex-scale modeling of denitrification. Representative modeling of denitrification will require accounting for particle growth along sedimentation trajectories, thereby convolving the temporal and spatial coordinates of the winter vortex in a detailed way.

Critically lacking for representative modeling of denitrification is an identified and verified nucleation process for this newly identified class of large particles. If nucleation involves preexisting particles, the process must effect a high selectivity because background aerosol number concentrations are near 10 cm^{-3} in the lower stratosphere (D > 0.008 μm) (*27, 28*), whereas the computed large-particle concentration in interval 2 is near 10^{-4} cm^{-3}. Selectivity is the key to the growth of the large-particle population observed here and their denitrification potential. If all available background particles grew and took up typical stratospheric HNO_3 amounts as NAT (or NAD), the average particle diameter would be <1 μm, and the sedimentation speed of individual particles would be <0.1 km day^{-1} (*13*). This speed is not adequate to explain significant denitrification as observed in both polar regions (*13, 14, 29*). Selectivity could be the consequence of (i) a very low freezing rate of background particles to form NAT (or NAD) at temperatures below ~197 K (*30, 31*), (ii) the unique composition of a few nuclei (*32, 33*), or (iii) ice formation (*10, 13, 34*) possibly involving lee-wave clouds (*10*).

Antarctic satellite observations show that denitrification occurs before dehydration as temperatures decrease in early winter (*29, 35*). The temporal separation of the HNO_3 and water removal processes could result if the large particles reported here also form in the Antarctic stratosphere before the onset of ice saturation temperatures. The more extensive low temperatures in the Antarctic suggest that large cles are formed there every winter, w their formation in the Arctic may not occ year. Before the 1999/2000 Arctic obser dilute populations of large particles in vortex may have eluded detection becaus able instruments did not sample the vort the appropriate times and places.

By the end of March 2000, large losses (up to 70% near 20 km) had oc in the lower stratosphere throughout th tic vortex (*23, 36*). The significant le denitrification observed throughout th tex is expected to have enhanced the cal loss (*36*). Arctic ozone abundanc remain vulnerable to increased winter loss in the coming decades as anthrop chlorine compounds are gradually re from the atmosphere, particularly if concentrations of greenhouse gases cooling in the polar vortex (*37*) and tr increasing water vapor continue in the stratosphere (*38*). Both effects incre extent of PSC formation and, thereby trification and the lifetime of active c (*29*). The role of large particles in ef denitrification in these future scena likely quite important. Substantial and spread denitrification could possibly chemical ozone loss in the Arctic e total chlorine levels fall below 2 p 2070 (*10*). In this case, recovery of ozone would be delayed until chlorin decline further. Models of denitrificat accurately represent the formation o particles will be required for accurate tions and understanding of future ozo els in the variable Arctic vortex.

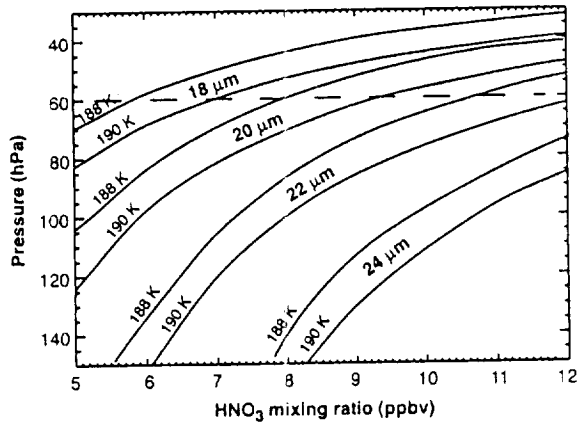

Fig. 6. Growth calculation results for maximum NAT particle diameter as a function of sampling pressure, HNO_3 mixing ratio, and temperature (*20*). Particles are assumed to grow and sediment in a one-dimensional atmospheric model defined by a constant temperature of 188 or 190 K, an H_2O mixing ratio of 5 ppmv, and a given HNO_3 mixing ratio (horizontal axis). Particle growth occurs wherever NAT supersaturation conditions exist and, hence, begins at pressures between 13 and 23 hPa (*25*) for the highest and lowest HNO_3 mixing ratios, respectively, and extends down to the highest pressure shown (150 hPa). The solid curves indicate the constant HNO_3 mixing ratio and temperature values in the model that will produce the indicated particle diameter at a given pressure level (vertical axis). The horizontal dashed line is the ER-2 pressure level for sampling interval 2 in Fig. 2. NAD particles grow more slowly than NAT particles for the same HNO_3 partial pressure and, hence, would grow to smaller sizes (~20% less) for the same atmospheric conditions.

References and Notes

1. "Scientific Assessment of Ozone Depletio *Rep. 44* (World Meteorological Organizatic va, Switzerland, 1999).
2. S. Solomon, *Rev. Geophys.* **37**, 275 (1999).
3. Th. Peter, *Annu. Rev. Phys. Chem.* **48**, 785
4. R. J. Salawitch *et al.*, *Science* **261**, 1146 (1
5. R. W. Portmann *et al.*, *J. Geophys. Res.* 10 (1996).
6. O. B. Toon *et al.*, *Geophys. Res. Lett.* **13**, 128
7. D. W. Fahey *et al.*, *Nature* **344**, 321 (1990
8. M. L. Santee, C. L. Manney, L. Froidevaux, W J. W. Waters, *J. Geophys. Res.* **104**, 8225 (
9. C. P. Rinsland *et al.*, *J. Geophys. Res.* **104**, 18
10. A. E. Waibel *et al.*, *Science* **283**, 2064 (199
11. Y. Kondo, H. Irie, M. Koike, G. E. Bodeker, *Res. Lett.* **27**, 337 (2000).
12. D. W. Fahey *et al.*, *J. Geophys. Res.* **94**, 112
13. R. J. Salawitch, G. P. Gobbi, S. C. Wofsy, M. B *Nature* **339**, 525 (1989).
14. O. B. Toon, R. P. Turco, P. Hamill, *Geophys.* **17**, 445 (1990).
15. The flights were part of the joint SAGE III C and Validation Experiment (SOLVE)/Third Stratospheric Experiment on Ozone 2000 2000) campaigns that took place in Kiruna, the 1999/2000 winter (additional informat o campaigns is available at http://cloud1.ar solve/ and www.nilu.no/projects/theseo200
16. In addition to the NO_y instrument, a che ization mass spectrometer (CIMS) detecte large PSC particles, and a multiangle aer trometer probe (MASP) measured the size ber concentration of large PSC particles

2000 with three instruments on board NASA ER-2 high-altitude aircraft as it the lower stratosphere inside the Arc- vortex (Fig. 1) (*15, 16*). Two instruments sured NO_y and HNO_3, respectively, in the gas phase and in aerosols, and one sured the size and number concentration ividual particles. The presentation here sed primarily on the NO_y instrument, has two independent measurement nels in order to distinguish sizes greater less than ~2 μm in diameter ("front" and NO_y data, respectively) (Fig. 2).

most extensive population of large icles was observed at aircraft cruise alti- 16 to 21 km) on 20 January 2000 a flight between Kiruna, Sweden, and North Pole (Figs. 1 and 2). Isolated peaks front NO_y data (Fig. 2C) at the begin- and end of the flight represent the sam- of individual HNO_3-containing parti- Throughout most of the flight, however, front NO_y data show a continuous series eaks (Fig. 2D) due to the sampling of a er number concentration of particles. The equivalent sphere diameter associated an individual particle peak can be cal- ated if typical PSC particle compositions assumed (*17*). The most likely solid phas- to form below 200 K are nitric acid trihy- ($HNO_3 \cdot 3H_2O$) (NAT) and nitric acid hydrate ($HNO_3 \cdot 2H_2O$) (NAD) (*3, 18, 19*). ngle large particles are unlikely to be liquid ercooled ternary solution (STS) composed HNO_3, H_2O, and H_2SO_4 (*20*). For a single icle composed of NAT, the relation be- en diameter D and the recorded NO_y val- is $D(\mu m) = 4.7\ [NO_y\ (ppbv)]^{1/3}$ (ppbv, s per billion by volume). Thus, the data in suggest that particles of sizes much ater than 2 μm in diameter were present over large horizontal regions (1800 km) in the center of the Arctic vortex. The presence of large particles is confirmed by the direct HNO_3 and aerosol size measurements (*16*).

The NO_y observations raise three questions. First, how can the size and number concentration be determined for these large HNO_3-containing particles? Second, do these

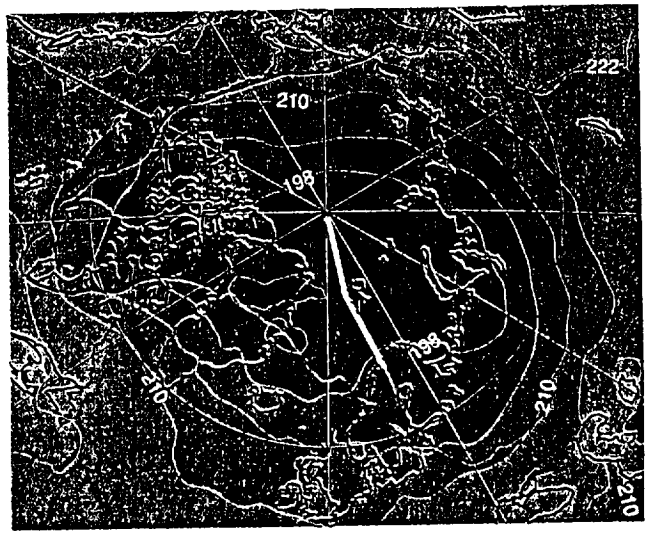

Fig. 1. Map of the ER-2 ground track on the flight of 20 January 2000 (yellow line) beginning in Kiruna, Sweden (67°N), reaching a maximum latitude of 89°N, and returning to Kiruna. The temperature field is shown by color shading and labeled contours (in K) on the 430 K isentropic surface (~19 km) at 1200 UTC on 20 January. The edge of the Arctic vortex (red contour) is defined by a potential vorticity value of 2.1×10^{-5} K m^2 kg^{-1} s^{-1}. The thick portion of the yellow line indicates that portion of the flight track where large particles were present.

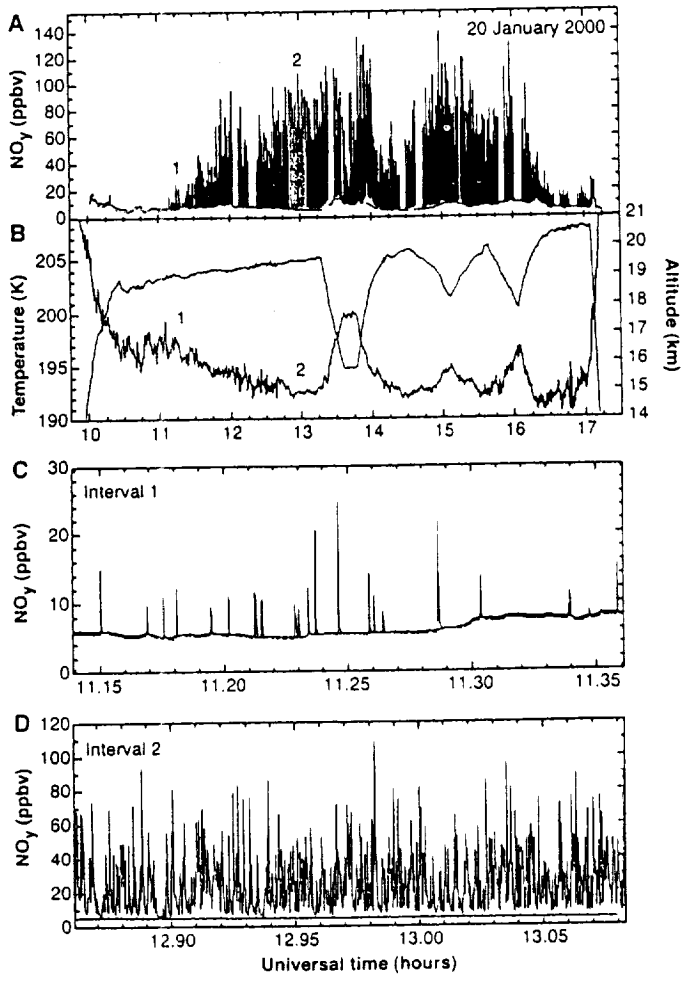

Fig. 2. Recorded data from the ER-2 flight of 20 January versus universal time (UT) corresponding to the flight track in Fig. 1. NO_y values from the front (black) and rear (red) inlets are shown for the entire flight in (A). Temperature (black) and altitude (red) are shown in (B). The 800-s intervals labeled in (A) as "1" (green) and "2" (blue) are expanded in (C) and (D), respectively. The data gaps in (A) correspond to instrument calibration periods. The aircraft speed is 0.2 km s^{-1}. The two NO_y measurements are made with inlets located front and rear, respectively, on a particle separator attached to the aircraft fuselage (*12, 43*). Air entering the front NO_y inlet contains particles of all sizes present, whereas air entering the rear NO_y inlet is inertially stripped of particles with diameters greater than ~2 μm. The separator does not affect the sampling of gas-phase species. Sampled particles are heated to 40°C along with sampled air, ensuring the release of condensed HNO_3 (and H_2O). Released HNO_3 is measured together with gas-phase HNO_3 through catalytic conversion to NO, which is subsequently detected by NO/O_3 chemiluminescence (*12*).

nomy Laboratory, [2]Climate Monitoring and Di- stics Laboratory, National Oceanic and Atmo- ic Administration, Boulder, CO 80305, USA. [3]Co- ative Institute for Research in Environmental Sci- s, University of Colorado, Boulder, CO 80309, School of the Environment, University of Leeds, S2 9JT, UK. [5]Rutherford Appleton Laboratory, on, Didcot, OX 11 0QX, UK. [6]Universidad Nacio- Autónoma de México, Centro de Ciencias de la osfera, Ciudad Universitaria, 04510 Mexico DF, co. [7]National Center for Atmospheric Research, der, CO 80307, USA. [8]Division of Geology and etary Sciences, [9]Division of Engineering and Ap- Science, California Institute of Technology, Pas- a, CA 91125, USA. [10]Laboratorium für Atmo- enphysik, Eidgenössiche Technische Hochs- Zürich, CH-8093 Zürich, Switzerland. [11]NASA Propulsion Laboratory, Pasadena, CA 91109, [12]NASA Ames Research Center, Moffett Field, 94035, USA. [13]Bay Area Environmental Research tute, San Francisco, CA 94122, USA. [14]Depart- of Engineering, University of Denver, Denver, 80208, USA. [15]Institute of Environmental ics, University of Bremen, D-28334 Bremen, many.

whom correspondence should be addressed. E- fahey@al.noaa.gov

cation of the Arctic vortex in a given winter depends on the spatial and temporal extent of sedimenting particle populations. If a flux value of 2.6 ppbv km day^{-1} were to be sustained for a period of only days near 20 km in a column model, a significant fraction (>50%) of available HNO_3 above 20 km would be removed.

Between 20 January and 7 March, large HNO_3-containing particles were present in additional sampling flights inside the Arctic vortex. The number and spatial extent of particles observed on these later flights were significantly less than those observed on 20 January. As the stratosphere warmed above NAT saturation temperatures by mid-March, large particles no longer appeared in the NO_y. On these later flights, two sampling periods contained particle populations that were notably different from those observed on 20 January. Both periods occurred at altitudes between 15 and 16 km. On 31 January, a 10-s burst of large particles was sampled with an average NO_y difference value many times that of interval 2. With diameters estimated to be near 20 μm, the instantaneous HNO_3 flux far exceeds that found in interval From the 3 February flight, the analysis of a 800-s interval shows a population of primarily 12-μm-diameter particles with concentrations near 10^{-3} cm^{-3} and an estimated flux comparable to that of interval 2.

Denitrification was widespread in the 1999/2000 Arctic winter, as estimated with in situ NO_y measurements and the NO_y-N_2O correlation as a reference (*7*, *22*). Denitrification exceeded 50% in many sampled air parcels in the 16- to 21-km altitude range throughout the vortex from January to March period, including most of the 20 January flight. Widespread denitrification was also found in satellite observations (*23*). The unusually low stratospheric temperatures in this Arctic winter, beginning in December, increased the likelihood of PSC formation and vortex denitrification (*24*). The different large-particle populations described here all contributed to vortex denitrification through PSC formation and sedimentation. It is likely, given the low winter temperatures, that similar populations present before 20 January further contributed to observed denitrification.

In answer to the third question, as to how large particles form in the lower stratosphere, we note that NAT particles above 10 μm in diameter found between 16 and 21 km must begin their growth and sedimentation at substantially higher altitudes. The altitude displacement is a function of growth rate and sedimentation velocity. To demonstrate how large particle sizes in Fig. 4 evolved after nucleation, we calculated sedimentation trajectories backward in time for particles observed in interval 2 (Fig. 5). Growing particles are advected by atmospheric winds and, hence, will be transported horizontally and vertically while they gravitationally sediment. The trajectory calculations take into account air parcel advection simultaneously with particle growth and sedimentation. The time evolution of particle size, pressure altitude, temperature, and NAT supersaturation ratio for particle sizes between 6 and 18 μm in diameter shows several important features (Fig. 5). First, the trajectories for all sizes terminate (reach zero size) in NAT-supersaturated air, indicating that the observed sizes are consistent with atmospheric and microphysical constraints of the trajectory model. Air masses encountered by particles must have temperatures that cause NAT supersaturation (short times at higher temperatures can be survived if particles are large enough). Second, growth of the largest particle requires 6 days and an ~6-km vertical displacement at temperatures below NAT saturation values. Third, the trajectories terminate at different altitudes, temperatures, and NAT supersaturation values. The horizontal locations of the termination points also vary (*25*). These preliminary results suggest that there are no obvious preferred locations or saturation conditions for nucleating the NAT particles observed in interval 2. The accumulation of HNO_3 in large particles in interval 2 causes some denitrification over the range of terminal altitudes. Finally, the trajectory temperatures at the start of particle growth (188 to 194 K) are above ice saturation by a few degrees. However, given the uncertainty in the meteorological analyses and atmospheric variability, ice saturation could have occurred along or near the trajectories and possibly played a role in particle nucleation. Particle trajectories also were calculated forward in time for interval 2. The results show that a 20-μm particle would continue to grow for another day, reach a maximum diameter of 22 μm at 150 hPa, and then evaporate (causing nitrification) within a few hours. Many instances of nitrification (NO_y in excess of the reference value) were observed in the vortex on the ER-2 flights.

Isolated particles sampled in interval 1 were significantly smaller than the mean size found in interval 2 (Fig. 2). The results of a similar particle trajectory analysis for interval 1 are consistent with the observed maximum size of ~13 μm in diameter. Although the trajectory analysis can account for such differences in size between different locations, it

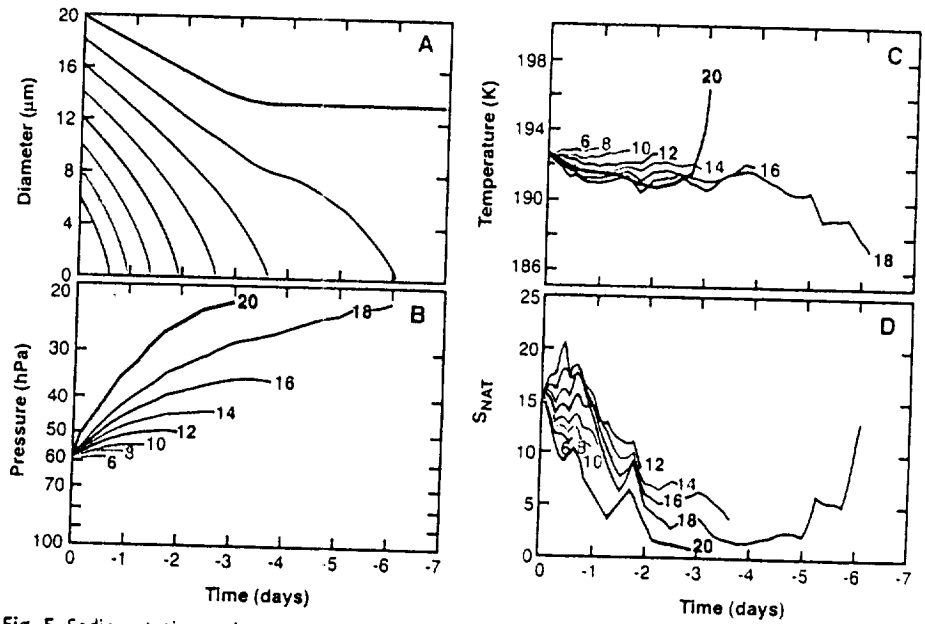

Fig. 5. Sedimentation trajectory calculations for different size particles present in interval 2 of Fig. 2. Trajectories simultaneously account for sedimentation, growth, and advection of a particle backward in time from interval 2. Trajectories for various particle sizes between 6 and 18 μm in diameter at day 0 are shown with colored lines and labeled by diameter. The results for (**A**) size, (**B**) pressure, (**C**) temperature, and (**D**) HNO_3 supersaturation ratio with respect to NAT (S_{NAT}) at the particle location are shown versus time (in days). The trajectories terminate where the particle diameter reaches zero. The trajectories were calculated by superimposing the particle vertical displacements due to sedimentation onto isentropic trajectories calculated with analyzed winds from the European Centre for Medium-Range Weather Forecasts. An H_2O mixing ratio of 5 ppmv and an HNO_3 mixing ratio of 7 ppbv were assumed, the latter being consistent with remote sounding observations (7 to 9 ppbv averaged above ER-2 altitudes) in mid-January 2000 (*26*). Temperatures remain above ice saturation for all particles. Particles with diameters greater than ~18 μm (or 20 μm at 9 ppbv HNO_3) had diameters greater than zero at the point where their trajectories exceeded the NAT equilibrium temperature and, thus, could not be present in interval 2 if growth began at the zero-size limit.

The Indian Ocean Experiment: Widespread Air Pollution from South and Southeast Asia

J. Lelieveld,[1]* P. J. Crutzen,[1,2] V. Ramanathan,[2] M. O. Andreae,[1] C. A. M. Brenninkmeijer,[1] T. Campos,[3] G. R. Cass,[4] R. R. Dickerson,[5] H. Fischer,[1] J. A. de Gouw,[6] A. Hansel,[7] A. Jefferson,[8] D. Kley,[9] A. T. J. de Laat,[6] S. Lal,[10] M. G. Lawrence,[1] J. M. Lobert,[2] O. L. Mayol-Bracero,[1] A. P. Mitra,[11] T. Novakov,[12] S. J. Oltmans,[8] K. A. Prather,[13] T. Reiner,[1] H. Rodhe,[14] H. A. Scheeren,[6] D. Sikka,[15] J. Williams[1]

The Indian Ocean Experiment (INDOEX) was an international, multiplatform field campaign to measure long-range transport of air pollution from South and Southeast Asia toward the Indian Ocean during the dry monsoon season in January to March 1999. Surprisingly high pollution levels were observed over the entire northern Indian Ocean toward the Intertropical Convergence Zone at about 6°S. We show that agricultural burning and especially biofuel use enhance carbon monoxide concentrations. Fossil fuel combustion and biomass burning cause a high aerosol loading. The growing pollution in this region gives rise to extensive air quality degradation with local, regional, and global implications, including a reduction of the oxidizing power of the atmosphere.

Until recently, North America and Europe dominated the use of fossil fuels, resulting in strong carbon dioxide emissions and global warming (*1*). The fossil energy–related CO_2 release per capita in Asia is nearly an order of magnitude smaller than in North America and Europe (*2*). However, Asia is catching up. About half of the world's population lives in South and East Asia, and hence the potential for growing pollutant emissions is large. In China, many pollution sources reduce air quality (*3–5*). In rural residential areas, notably in India, the burning of biofuels, such as wood, dung, and agricultural waste, is a major source of pollutants (*6*). In urban areas, the increasing energy demand for industry and transport propels fossil fuel utilization (*7*).

Here we evaluate measurements of the Indian Ocean Experiment (INDOEX) to characterize the atmospheric chemical composition of the outflow from South and Southeast Asia, from January to March 1999 during the dry winter monsoon (*8*). During this season, the northeasterly winds are persistent, and convection over the continental source regions is suppressed by large-scale subsidence, thus limiting upward dispersion of pollution (*9*). Our analysis is based on measurements from a C-130 and a Citation aircraft operated from the Maldives near 5°N, 73°E, the research vessels *Ronald H. Brown* and *Sagar Kanya*, and the Kaashidhoo Climate Observatory (KCO) on the Maldives (Fig. 1). During the campaign, the location of the Intertropical Convergence Zone (ITCZ) varied between the equator and 12°S. Hence, transport of primary pollutants and reaction products toward the ITCZ could be studied over an extended ocean area where pollutant emissions are otherwise minor. By performing measurements across the ITCZ, the polluted air masses could be contrasted against comparatively clean air over the southern Indian Ocean. Furthermore, we used the measurements to evaluate the numerical representation of these processes in a chemistry general circulation model (GCM) (*10*). The model was subsequently applied to calculate the large-scale atmospheric chemical effects of the measured pollution.

Aerosol chemical and optical measurements were performed from both aircraft, the R/V *Brown*, and KCO. The latter is located

[1]Max-Planck-Institute for Chemistry, Post Office Box 3060, D-55020 Mainz, Germany. [2]Center for Atmospheric Sciences, Scripps Institution of Oceanography, La Jolla, CA 92093–4922, USA. [3]National Center for Atmospheric Research, Boulder, CO 80303, USA. [4]School of Earth and Atmospheric Sciences, Georgia Institute of Technology, Atlanta, GA 30332–0340, USA. [5]Department of Meteorology, University of Maryland, College Park, MD 20742, USA. [6]Utrecht University, 3584 CC Utrecht, Netherlands. [7]University of Innsbruck, A-6020 Innsbruck, Austria. [8]Climate Monitoring and Diagnostics Laboratory, National Oceanic and Atmospheric Administration, Boulder, CO 80303, USA. [9]Research Centre Jülich, ICG-2, D-52428, Jülich, Germany. [10]Physical Research Laboratory, Navrangpura, Ahmedabad 380 009, India. [11]National Physical Laboratory, New Delhi 110 012, India. [12]Lawrence Berkeley National Laboratory, Berkeley, CA 94720, USA. [13]University of California, Riverside, CA 92521–0403, USA. [14]Department of Meteorology, Stockholm University, S-10691 Stockholm, Sweden. [15]40 Mausam Vihar, New Delhi 110051, India.

*To whom correspondence should be addressed. E-mail: lelieveld@mpch-mainz.mpg.de

GEOPHYSICAL RESEARCH LETTERS, VOL. 28, NO. 15, PAGES 2875-2878, AUGUST 1, 2001

Severe and Extensive Denitrification in the 1999-2000 Arctic Winter Stratosphere

P.J. Popp[1,2], M.J. Northway[1,2], J.C. Holecek[1,2], R.S. Gao[1], D.W. Fahey[1,2], J.W. Elkins[3], D.F. Hurst[3,2], P.A. Romashkin[3,2], G.C. Toon[4], B. Sen[4], S.M. Schauffler[5], R.J. Salawitch[4], C.R. Webster[4], R.L. Herman[4], H. Jost[6], T.P. Bui[6], P.A. Newman[7], L.R. Lait[7]

Abstract. Observations in the 1999-2000 Arctic winter stratosphere show the most severe and extensive denitrification ever observed in the northern hemisphere. Denitrification was inferred from *in situ* measurements conducted during high-altitude aircraft flights between January and March 2000. Average removal of more than 60% of the reactive nitrogen reservoir (NO_y) was observed in air masses throughout the core of the Arctic vortex. Denitrification was observed at altitudes between 16 and 21 km, with the most severe denitrification observed at 20 to 21 km. Nitrified air masses were also observed, primarily at lower altitudes. These results show that denitrification in the Arctic lower stratosphere can approach the severity and extent of that previously observed only in the Antarctic.

Introduction

Denitrification, defined as the permanent removal of NO_y from an air mass by the sedimentation of polar stratospheric cloud (PSC) particles, can slow chlorine deactivation and thereby enhance polar ozone loss [*Fahey et al.*, 1990; *Rex et al.*, 1997]. Polar stratospheric clouds contain nitric acid (HNO_3), the principal component of stratospheric NO_y. Severe (>50% NO_y removal) and geographically extensive denitrification in the Antarctic lower stratosphere is a well-known phenomenon [*Fahey et al*, 1990; *Fahey et al.*, 1989a; *Santee et al.*, 1999]. The degree to which the Arctic stratosphere denitrifies is more variable, however, due to generally warmer temperatures that result in shorter PSC lifetimes [*Fahey et al.*, 1990; *Santee et al.*, 1999; *Tabazadeh et al.*, 2000]. Thus far, observations of denitrification in the Arctic vortex have been limited to those made by satellites and infrequent *in situ* sampling from aircraft and balloon platforms [*Fahey et al.*, 1990; *Santee et al.*, 1999; *Sugita et al.*, 1998; *Kondo et al.*, 2000]. While severe denitrification has been inferred from the *in situ* measurements for localized regions of the Arctic, [*Fahey et al.*, 1990; *Sugita et al.*, 1998], these observations are not considered representative of the entire vortex. Although NO_y removal that is both severe and widespread has not been observed previously in the Arctic, the region is arguably at the threshold for such denitrification [*Waibel et al.*, 1999]. The observations presented here show the 1999-2000 Arctic winter crossing the threshold for Antarctic-like denitrification.

Results and Discussion

In situ measurements of NO_y, by catalytic reduction/chemiluminescence [*Fahey et al.*, 1989b], and nitrous oxide (N_2O), by gas chromatography [*Romashkin et al.*, 2001], were conducted in the Arctic vortex during 11 flights of the NASA ER-2 aircraft between 20 January and 12 March 2000. These flights were performed as part of the joint SAGE III Ozone Loss and Validation Experiment (SOLVE)/Third European Stratospheric Experiment on Ozone (THESEO) 2000 campaigns in Kiruna, Sweden (68° N, 20° E). Denitrification is quantified using the correlation between the measured NO_y and N_2O mixing ratios (reported every 70s) as shown in Fig. 1a. The reference value of NO_y, NO_y^*, is given by the NO_y-N_2O correlation established using remote measurements obtained by the MkIV balloon-borne interferometer [*Toon*, 1991] in the 1999-2000 Arctic vortex prior to the onset of denitrification (solid line in Fig. 1a).

The aircraft data show severe denitrification between late January and mid-March, at altitudes from 17 to 21 km, and for N_2O levels between 40 and 170 ppbv (Fig. 1a). All air masses observed with N_2O levels less than 125 ppbv (encountered on 10 of 11 ER-2 flights) were denitrified. The most severely denitrified air masses showed residual NO_y levels (NO_y remaining in a denitrified air mass) of less than 3 ppbv, resulting from more than 80% of the NO_y being removed. Data points above the NO_y^* reference line in Fig. 1a indicate nitrification, thought to be caused by the evaporation of PSC particles that have sedimented from higher altitudes. To exclude measurements made when NO_y-containing PSC particles were present in the sampled air mass, the *in situ* data shown in Fig. 1a (and throughout) represent observations made at temperatures greater than the threshold temperature for the formation of nitric acid trihydrate (T_{NAT}). Values of T_{NAT} were calculated continuously using *in situ* measurements of NO_y (as equivalent HNO_3), water vapor, and pressure. Excluding these measurements ensures that NO_y is irreversibly removed from the denitrified air mass, and not partially sequestered in particle form. Residual NO_y levels as low as 0.9 ppbv were also observed, although these measurements were made in air masses below PSC formation temperatures (data not shown).

Remote measurements of NO_y reported for a flight of the MkIV interferometer on 15 March 2000 show up to 40% denitrification at 19-20 km, in comparison to the 3 December 1999 flight used to establish the NO_y^* reference state (Fig. 1b). These denitrifications are less than those measured onboard the ER-2, particularly for values of N_2O < 100 ppbv. Although the 15

[1]Aeronomy Laboratory, National Oceanic and Atmospheric Administration, Boulder, CO
[2]Cooperative Institute for Research in Environmental Sciences, University of Colorado, Boulder, CO
[3]Climate Monitoring and Diagnostics Laboratory, National Oceanic and Atmospheric Administration, Boulder, CO
[4]NASA Jet Propulsion Laboratory, Caltech, Pasadena, CA
[5]National Center for Atmospheric Research, Boulder, CO
[6]NASA Ames Research Center, Moffett Field, CA
[7]NASA Goddard Space Flight Center, Greenbelt, MD

Paper number 2001GL013132.
0094-8276/01/2001GL013132$05.00

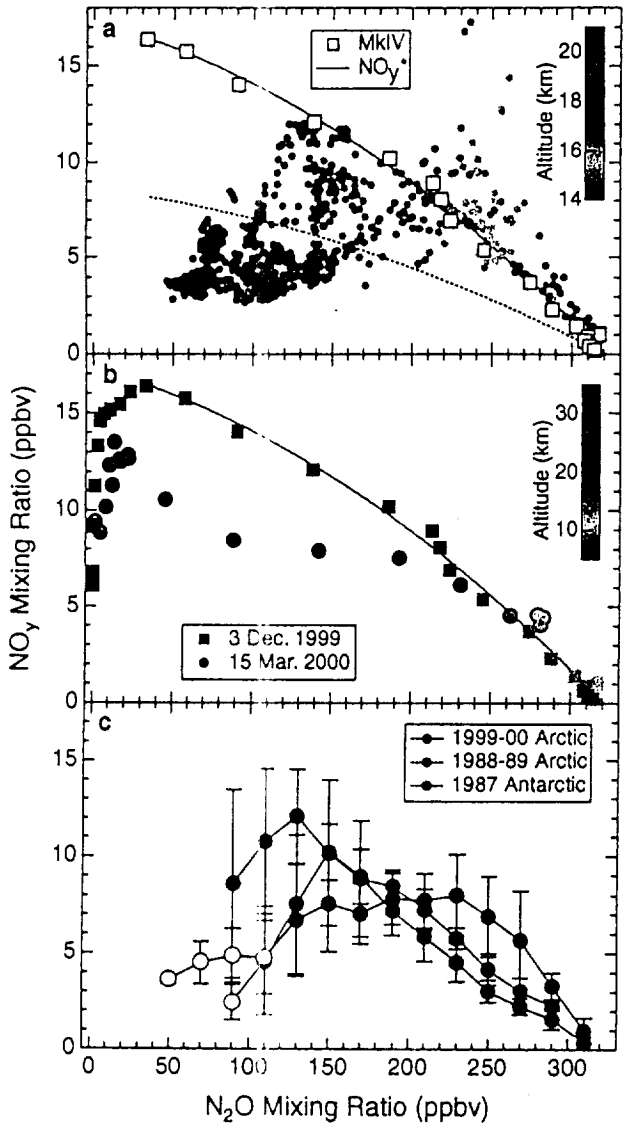

Figure 1. (a) NO_y-N_2O scatter plot for data measured during 11 flights of the NASA ER-2. Data are colored as a function of the altitude at which the individual measurements were made. Unfilled squares represent measurements made by the MkIV balloon-borne interferometer prior to the onset of denitrification, flown inside the Arctic vortex from Esrange, Sweden (68° N, 20° E) on 3 December 1999. The NO_y^* reference state was determined from a third-order polynomial fit to the MkIV data, given by

$$NO_y^* = 17.3 - (0.0222 \cdot N_2O) - (9.85 \cdot 10^{-5}) \cdot (N_2O)^2$$

for N_2O values between 33 and 321 ppbv. The dotted line represents 50% of the value of NO_y^*, indicating the difference between moderate and severe denitrification. (b) NO_y-N_2O scatter plot for data reported by the MkIV interferometer during balloon flights on 3 December 1999 and 15 March 2000. Data are colored as a function of the altitude at which the measurements were reported. The black line represents the NO_y^* reference state shown in panel (a). (c) Composite NO_y-N_2O scatter plot for the ER-2 data shown in panel (a) (blue symbols). Similar treatments of the data are shown for 7 flights of the Airborne Antarctic Ozone Experiment in 1987 (red symbols) and 8 flights of the Airborne Arctic Stratospheric Expedition in 1988-89 (green symbols). Bins showing severe denitrification are represented by unfilled symbols. Bars show the standard deviation of the data within each N_2O bin, and are not intended to represent the uncertainty in the mean NO_y value.

March MkIV 2000 observations were obtained at high equivalent latitudes, the tracer-potential temperature relationships observed during this flight were more representative of the vortex edge than the vortex core, which might explain the lower values of denitrification inferred from the MkIV measurements. Alternatively, the differences could arise from the different sampling characteristics (i.e. vertical resolution, altitude ceiling) of the remote and *in situ* data.

Mixing can produce air masses with NO_y-N_2O relationships that deviate from the NO_y^* reference state because of the nonlinearity of the NO_y-N_2O correlation at low values of N_2O [Rex *et al.*, 1999]. These air masses can result from isentropic mixing of air across the edge of the vortex, or from isentropic mixing of air masses within the vortex that have undergone non-uniform descent. Without knowledge of such mixing, air parcels which deviate from the reference state could be described incorrectly as having been denitrified. The initial relationship between NO_y and N_2O measured inside the Arctic vortex by the MkIV interferometer on 3 December, 1999 (Fig. 1b) shows that the near-linear portion of the initial reference state in the Arctic vortex extends to lower values of N_2O (~20 ppbv) than had previously been as-

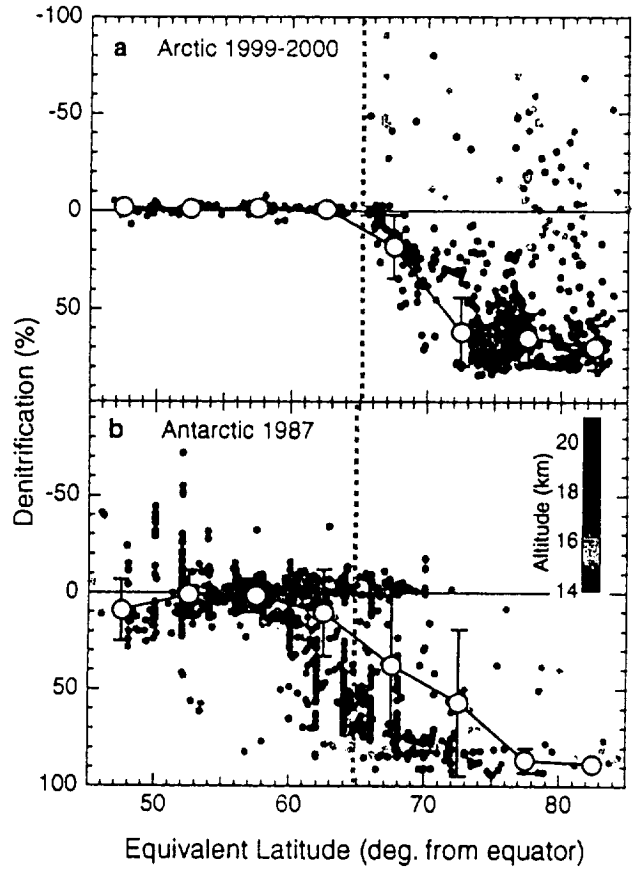

Figure 2. (a) Denitrification as a function of equivalent latitude observed during 11 flights of the NASA ER-2. Positive values of denitrification represent NO_y removal. Unfilled black symbols represent mean denitrification values for measurements made at altitudes between 18 and 21 km. Error bars show the standard deviation of the data within each equivalent latitude bin. The dashed line at 65.2° N represents the mean equivalent latitude of the vortex edge (defined by potential vorticity) during the 11 ER-2 flights. (b) Same as Fig. 2a for 6 Antarctic vortex flights of the NASA ER-2 between August 30 and September 22, 1987. Unfilled black symbols represent mean denitrification values for measurements made at altitudes between 16 and 21 km. The dashed line at 64.9° S represents the mean equivalent latitude of the vortex edge during the 6 ER-2 flights.

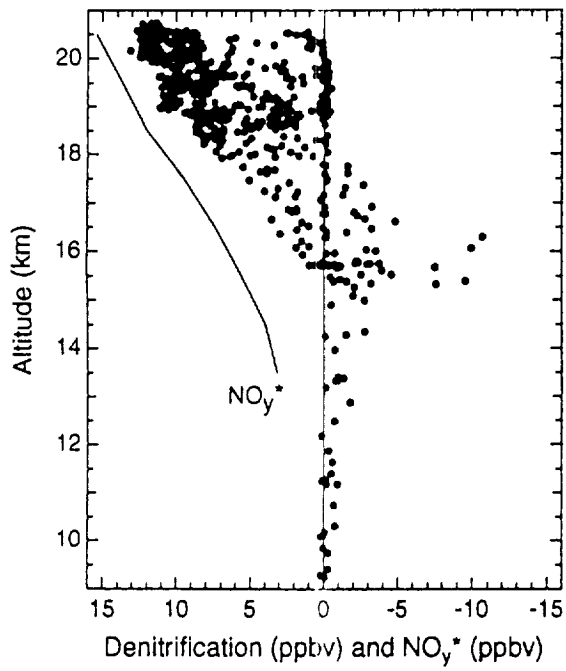

Figure 3. Vertical profile of redistributed NO_y in the 1999-2000 Arctic vortex. Positive values of denitrification represent NO_y removal. Blue and red symbols represent measurements made at greater than 70° N and less than 70° N equivalent latitude, respectively. The solid black line representing NO_y^* was determined from altitude bin-averaged N_2O values for measurements made throughout the winter at equivalent latitudes greater than 70° N. This term represents the maximum available NO_y at a given altitude. Maximum ER-2 flight altitudes of 20-21 km represent a potential temperature of approximately 460-475 K.

sumed (~40-50 ppbv) by Rex *et al.* [1999]. This feature makes it unlikely that transport and mixing substantially altered the NO_y^* reference state from that shown in Figs. 1a and 1b. The *in situ* data set of long-lived trace gases obtained by the Observations of the Middle Stratosphere (OMS) balloon gondola during two flights above Kiruna also indicate that mixing did not significantly alter the NO_y-N_2O relationship during this winter.

Studies of PSC climatology show that consistently cold temperatures characteristic of the Antarctic vortex are highly favorable for the formation and sedimentation of PSCs [*Poole and Pitts*, 1994]. Temperatures in the Arctic winter stratosphere, however, are typically warmer and more variable from year to year, resulting in a lower probability of PSC formation and denitrification [*Poole and Pitts*, 1994]. These temperature patterns are consistent with previous *in situ* measurements of NO_y and N_2O [*Loewenstein et al.*, 1989] that show more extensive denitrification for the 1987 Antarctic winter than for the 1988-89 Arctic winter (Fig. 1c). While the 1988-89 Arctic data show evidence of only moderate NO_y loss, the 1987 Antarctic data set indicates the onset of severe denitrification at N_2O levels less than 130 ppbv. Satellite data collected by the Microwave Limb Sounder (MLS) in more recent years also show more denitrification in the Antarctic vortex compared to the Arctic [*Santee et al.*, 1999].

When the 1988-89 and 1999-2000 Arctic data are compared, there is a significant difference in the inferred denitrification (Fig. 1c). In 1999-2000, denitrification occurs over a broader range of N_2O values, the onset of NO_y loss occurs at higher N_2O values (190 ppbv), and mean residual NO_y levels fall below 5 ppbv at the lowest values of N_2O. In comparison to the Antarctic data set, the 1999-2000 Arctic data reveal denitrification over a broader range of N_2O values, and slightly more loss of NO_y between N_2O values of 110 and 170 ppbv. Only at the lowest values of N_2O common to all three data sets (90-110 ppbv) does the Antarctic data show more removal of NO_y. Thus, the severity of denitrification in the 1999-2000 Arctic vortex is comparable to that inferred from previous *in situ* measurements in the Antarctic polar vortex. The high values of NO_y between 230 and 290 ppbv N_2O in the 1999-2000 Arctic data are due to the nitrified air masses at altitudes between 15 and 17 km (see Fig. 1a).

In addition to causing denitrification, Antarctic temperatures are consistently low enough to cause dehydration via the sedimentation of ice particles. Satellite observations in the Antarctic vortex suggest that denitrification occurs before dehydration as temperatures decrease during the early winter [*Santee et al.*, 1995]. *In situ* measurements of water vapor [*May*, 1998] were obtained during all flights of the NASA ER-2 in the 1999-2000 Arctic vortex. Denitrification was not accompanied by any significant dehydration in this data set except briefly during the flight of 27 January 2000, consistent with the permanent removal of NO_y at temperatures above the formation threshold for ice particles.

The severe denitrification in the 1999-2000 Arctic stratosphere was observed throughout the core of the vortex. In Fig. 2a fractional denitrification is shown as a function of the equivalent (vortex-normalized) latitude [*Nash et al.*, 1996] of the measurements. An equivalent latitude of 90° corresponds to the center of the vortex. Mean denitrification values, at altitudes between 18 and 21 km, indicate that more than 60% of the expected NO_y was removed from air masses sampled at equivalent latitudes between 70° and 85° N (black symbols in Fig. 2a). The most severely denitrified air masses, with more than 80% of the expected NO_y removed, were observed poleward of 73° N. Negative values in Fig. 2a indicate nitrified air masses, observed over the same range of equivalent latitudes but at lower altitudes. A similar treatment of the data for *in situ* measurements obtained in the 1987 Antarctic vortex is shown in Fig. 2b. The most severely denitrified air masses observed in the Antarctic show more than 90% of the NO_y being removed at equivalent latitudes greater than 65° S, with mean denitrification values between 16 and 21 km (black symbols in Fig. 2b) exceeding 80% poleward of 75° S. Figure 2 shows a striking similarity between the severity and extent of denitrification in the Arctic and Antarctic vortices in the observed years, with the Antarctic data set showing more severe denitrification over a greater range of equivalent latitudes. The apparent denitrification (and nitrification) at equivalent latitudes less than 55° S in Fig. 2b occurs in air masses containing low values of NO_y, for which small deviations from the NO_y^* reference state can cause large fractional denitrification.

Severe denitrification over broad regions of the 1999-2000 Arctic vortex was not detected in MLS satellite measurements [*Santee et al.*, 2000]. The MLS data suggest that only 20% of the available HNO_3 was removed between equivalent latitudes of 70° and 80° N. Since the HNO_3/NO_y ratio generally exceeds 80%, percent denitrification is approximately equal to that of percent HNO_3 removal. The difference in the reported severity of denitrification in the 1999-2000 Arctic vortex may be due to the location, timing and vertical resolution (6 km) of the MLS HNO_3 measurements [*Santee et al.*, 2000], which causes denitrification to be reported as an average of many air parcels over a range of altitudes.

A vertical profile of denitrification in the 1999-2000 Arctic stratosphere reveals that NO_y removal was most intense in the vortex core at altitudes of 20-21 km (blue symbols in Fig. 3). Severe denitrification may have also occurred above 21 km, the maximum altitude attained by the ER-2. Below 21 km, maximum NO_y removal decreases with altitude down to 16 km, below which no denitrification was observed. This altitude dependence results from lower amounts of available NO_y at lower altitudes, as

indicated by the black line denoting NO_y^* in Fig. 3, and warmer temperatures (and thus decreased PSC activity) at lower altitudes. In addition, the denitrification observed in any given air mass reflects a balance between the NO_y removed from the air mass and any nitrification that has occurred. This conclusion is supported by the observation of some air masses between 15 and 17 km with higher than expected NO_y mixing ratios. Such nitrification has been observed previously in the Arctic polar vortex by both *in situ* [*Hubler et al.*, 1990] and remote methods [*Kondo et al.*, 2000].

Implications

Modeling studies have demonstrated that denitrification can significantly enhance ozone loss in polar spring [*Salawitch et al.*, 1993; *Rex et al.*, 1997; *Waibel et al.*, 1999; *Tabazadeh et al.*, 2000]. The enhancement is expected to be greatest in denitrified air masses for which temperatures are too high to maintain active chlorine levels via heterogeneous reprocessing [*Portmann et al.*, 1996]. Consequently, denitrification may play a more prominent role in ozone loss in the warmer Arctic spring, despite the typically higher levels of observed denitrification reported in the Antarctic [*Portmann et al.*, 1996]. Severe ozone loss was observed in the 1999-2000 Arctic winter stratosphere [*Sinnhuber et al.*, 2000; *Richard et al.*, 2001]. Modeling studies have partly attributed this enhanced ozone loss to a delay in chlorine deactivation caused by denitrification [*Sinnhuber et al.*, 2000]. The 1999-2000 Arctic vortex experienced temperatures below the formation threshold for PSC particles over a greater area than in any previously observed winter [*Manney and Sabutis*, 2000]. These cold temperatures were accompanied by denitrification in the lower stratosphere approaching the severity and extent of that previously observed only in the Antarctic. If the observed trend towards a colder Arctic stratosphere continues [*Shindell et al.*, 1998], severe and extensive denitrification and the associated enhanced ozone loss is likely. The observations in the 1999-2000 Arctic vortex provide an important example of the denitrification that may become more frequent in future colder Arctic winters.

Acknowledgements. We thank NASA ER-2 pilots J. Barrilleaux, J. Nystrom and D. Porter, and S.E. Strahan for providing the equivalent latitude data shown in Figure 2b. This work was supported by the NASA Upper Atmosphere Research Program.

References

Fahey, D.W. *et al.*, Measurements of nitric oxide and total reactive nitrogen in the Antarctic stratosphere: Observations and chemical implications, *J. Geophys. Res.*, *94*, 16665-16681, 1989a.

Fahey, D.W. *et al.*, In situ measurements of total reactive nitrogen, total water, and aerosol in a polar stratospheric cloud in the Antarctic, *J. Geophys. Res.*, *94*, 11299-11315, 1989b.

Fahey, D.W. *et al.*, Observations of denitrification and dehydration in the winter polar stratospheres, *Nature*, *344*, 321-324, 1990.

Hubler, G. *et al.* Redistribution of reactive odd nitrogen in the lower arctic stratosphere. *Geophys. Res. Lett.*, *17*, 453-456, 1990.

Kondo, Y., H. Irie, M. Koike, and G. E. Bodeker, Denitrification and nitrification in the Arctic stratosphere during the winter of 1996-1997, *Geophys. Res. Lett.*, *27*, 337-340, 2000.

Loewenstein, M., J. R. Podolske, K. R. Chan, and S. E. Strahan, Nitrous oxide as a dynamical tracer in the 1987 airborne Antarctic ozone experiment, *J. Geophys. Res.*, *94*, 11589-11598, 1989.

Manney, G.L. and J. L. Sabutis, Development of the polar vortex in the 1999-2000 Arctic winter stratosphere, *Geophys. Res. Lett.* 27, 2589-2592, 2000.

May, R.D., Open-path, near-infrared tunable diode laser spectrometer for atmospheric measurements of H_2O, *J. Geophys. Res.*, *103*, 19161-19172, 1998.

Nash, E.R., P. A. Newman, J. E. Rosenfield, and M. R. Schoeberl. An objective determination of the polar vortex using Ertel's potential vorticity, *J. Geophys. Res.*, *101*, 9471-9478, 1996.

Poole, L.R. and M. C. Pitts, Polar stratospheric cloud climatology based on Stratospheric Aerosol Measurement II observations from 1978 to 1989. *J. Geophys. Res.*, *99*, 13083-13089, 1994.

Portmann, R.W. *et al.*, Role of aerosol variations in anthropogenic ozone depletion in the polar regions, *J. Geophys. Res.*, *101*, 22991-23006, 1996.

Rex, M. *et al.*, Subsidence, mixing, and denitrification of Arctic polar vortex air measured during POLARIS, *J. Geophys. Res.*, *104*, 26611-26623, 1999.

Rex, M. *et al.*, Prolonged stratospheric ozone loss in the 1995-96 Arctic winter, *Nature*, *389*, 835-838, 1997.

Richard, *et al.*, Severe chemical ozone loss inside the Arctic polar vortex during winter 1999-2000 inferred from in-situ airborne measurements, *Geophys. Res. Lett.*, *28*, 2197-2200, 2001.

Romashkin, P.A. *et al.*, In situ measurements of long-lived trace gases in the lower stratosphere by gas chromatography, *J. Atmos. Oceanic Technol.*, *18*, 1195-1204, 2001.

Salawitch, R.J. *et al.*, Chemical loss of ozone in the Arctic polar vortex in the winter of 1991-1992, *Science*, *261*, 1146-1149, 1993.

Santee, M.L. *et al.*, Interhemispheric differences in polar stratospheric HNO_3, H_2O, ClO, and O_3, *Science*, *267*, 849-852, 1995.

Santee, M.L., G. L. Manney, L. Froidevaux, G. W. Read, and J. W. Waters, Six years of UARS microwave limb sounder HNO_3 observations: Seasonal, interhemispheric, and interannual variations in the lower stratosphere, *J. Geophys. Res.*, *104*, 8225-8246, 1999.

Santee, M.L., G. L. Manney, N. J. Livesey, and W. J. Waters, UARS Microwave Limb Sounder observations of denitrification and ozone loss in the 2000 Arctic late winter, *Geophys. Res. Lett.*, *27*, 3213-3216, 2000.

Shindell, D.T., D. Rind, and P. Lonergan, Increased polar stratospheric ozone losses and delayed eventual recovery owing to increasing greenhouse-gas concentrations, *Nature*, *392*, 589-592, 1998.

Sinnhuber, B.-M. *et al.*, Large loss of total ozone during the Arctic winter of 1999/2000, *Geophys. Res. Lett.*, *27*, 3473-3476, 2000.

Sugita, T. *et al.*, Denitrification observed inside the arctic vortex in February 1995, *J. Geophys. Res.*, *103*, 16221-16233, 1998.

Tabazadeh, A. *et al.*, Quantifying denitrification and its effect on ozone recovery, *Science*, *288*, 1407-1411, 2000.

Toon, G.C. The JPL MkIV Interferometer, *Opt. Photonics News*, 2, 19-21, 1991.

Waibel, A.E. *et al.*, Arctic ozone loss due to denitrification, *Science*, *283*, 2064-2069, 1999.

P. J. Popp, M. J. Northway, J. C. Holecek, R. S Gao, and D. W. Fahey, Aeronomy Laboratory, National Oceanic and Atmospheric Administration, Boulder, CO 80305 (e-mail: ppopp@al.noaa.gov)

J. W. Elkins, D. F. Hurst, and P. A Romashkin, Climate Monitoring and Diagnostics Laboratory, National Oceanic and Atmospheric Administration, Boulder, CO 80305

G. C. Toon, B. Sen, R. J. Salawitch, C. R. Webster, and R. L. Herman, NASA Jet Propulsion Laboratory, Caltech, Pasadena, CA 91109

S. M. Schauffler, National Center for Atmospheric Research, Boulder, CO 80307

H. Jost and T. P. Bui, NASA Ames Research Center, Moffett Field, CA 94035

P. A. Newman and L. R. Lait, NASA Goddard Space Flight Center, Greenbelt, MD 20771

(Received March 5, 2001; revised June 4, 2001;
accepted June 5, 2001)